The Astronomical Journal, 166:172 (19pp), 2023 October https://doi.org/10.3847/1538-3881/acf297

Mass Ratio of Single-line Spectroscopic Binaries with Visual Orbits Using Bayesian Inference and Suitable Priors*

Jennifer Anguita-Aguero[1], Rene A. Mendez[2], Miguel Videla[3], Edgardo Costa[1], Leonardo Vanzi[4], Nicolas Castro-Morales[5], and Camila Caballero-Valdes[1]
[1] Astronomy Department, Universidad de Chile, Casilla 36-D, Santiago, Chile; rmendez@uchile.cl
[2] Astronomy Department, Universidad de Chile, Casilla 36-D, Santiago, Chile and European Southern Observatory, Alonso de Córdova 3107, Vitacura Santiago, Chile
[3] Department of Electrical Engineering Information and Decision Systems Group (IDS), Facultad de Ciencias Físicas y Matemáticas, Universidad de Chile, Beauchef 850, Santiago, Chile
[4] Department of Electrical Engineering and Centre of Astro Engineering, Pontificia Universidad Católica de Chile, Av. Vicuña Mackenna 4860, Santiago
[5] Instituto de Astrofísica, Pontificia Universidad Católica de Chile, Instituto Milenio de Astrofísica (MAS), Av. Vicuña Mackenna 4860, Santiago
Received 2023 June 23; revised 2023 August 15; accepted 2023 August 17; published 2023 September 25

Abstract

We present orbital elements for 22 single-line binaries, nine of them studied for the first time, determined from a joint spectroscopic and astrometric solution. The astrometry is based on interferometric measurements obtained with the HRCam Speckle camera on the SOAR 4.1 m telescope at Cerro Pachon, Chile, supplemented with historical data. The spectroscopic observations were secured using Echelle spectrographs (FEROS, FIDEOS, and HARPS) at La Silla, Chile. A comparison of our orbital elements and systemic velocities with previous studies, including Gaia radial velocities, shows the robustness of our estimations. By adopting suitable priors of the trigonometric parallax and spectral type of the primary component, and using a Bayesian inference methodology developed by our group, we were able to estimate mass ratios for these binaries. Combining the present results with a previous study of other single-line binaries from our team, we present a pseudo mass-to-luminosity relationship based on 23 systems (46 stars) in the mass range $0.6 \leqslant M_{\odot} \leqslant 2.5$. We find a reasonable correspondence with a fiducial mass-to-luminosity relationship. We conclude that our methodology does allow us to derive tentative mass ratios for these types of binaries.

Unified Astronomy Thesaurus concepts: Binary stars (154); Astrometric binary stars (79); Visual binary stars (1777); Interferometric binary stars (806); Stellar masses (1614); Stellar properties (1624); Mass ratio (1012); Spectroscopic binary stars (1557); Bayesian statistics (1900); Posterior distribution (1926); Prior distribution (1927); Stellar luminosities (1609)

1. Introduction

Spectroscopic binaries are powerful astrophysical laboratories. Combining precise astrometric and radial velocity (RV) measurements for these systems, it is possible to obtain a fairly complete characterization of their orbital and basic astrophysical parameters. Among them, two groups are distinguished: double-line spectroscopic binaries (SB2s), in whose spectra the spectral lines of both components are distinguished, and single-line spectroscopic binaries (SB1s), for which only the lines of the primary component are easily recognized.

SB2s are certainly the most interesting systems, because in their case a joint treatment of the astrometric and RV data allows one to determine directly the individual component masses (Anguita-Aguero et al. 2022), as well as a parallax-free distance, allowing an independent assessment of Gaia's trigonometric parallaxes (Pourbaix 2000; Mason 2015).

Unfortunately, for SB1s, which are the majority (67%) of the systems included in the 9th Catalog of Spectroscopic Binary Orbits[6] (SB9; Pourbaix et al. 2004), only the mass function can be obtained directly[7] (Struve & Huang 1958). For this reason, in the past, this latter group has not been fully exploited.

Now, thanks to a newly developed Bayesian methodology based on the Markov Chain Monte Carlo (MCMC) algorithm, No-U-Turn sampler (Videla et al. 2022), for addressing the orbital parameter inference problem in SB1 systems, including an estimation of the individual component masses, this situation is rapidly changing. This scheme also provides a precise characterization of the uncertainty of the estimates of the orbital parameters, in the form of a joint posterior probability distribution function (PDF).

In this approach, the lack of an RV curve for the secondary star is managed by incorporating suitable prior distributions for two critical parameters of the system; namely, its trigonometric parallax (from an external source) and the mass of the primary component, estimated from its Spectral Type (SpTy). This methodology has been thoroughly tested on several benchmark SB2 systems by Videla et al. (2022), who provide an exhaustive analysis of the results obtained by comparing the PDFs from different observational sources and priors. In that

* Based in part on observations obtained at the Southern Astrophysical Research (SOAR) telescope, which is a joint project of the Ministério da Ciência, Tecnologia, e Inovaçãoes (MCTI) da República Federativa do Brasil, the U.S. National Optical Astronomy Observatory (NOAO), the University of North Carolina at Chapel Hill (UNC), and Michigan State University (MSU).

[6] Updated regularly, and available at https://sb9.astro.ulb.ac.be/.
[7] The mass function is defined by $f(M) = \frac{(m_s \sin i)^3}{(m_p + m_s)^2}$, where m_p and m_s are the mass of the primary and secondary stars, respectively.

paper, we were able to show that this Bayesian approach allows a much richer and more complete understanding of the associated uncertainties in the study of binary systems in general.

Here, we apply this methodology to 22 SB1 systems, nine of which (HIP 29860, 36497, 38414, 40167, 54061, 76031, 93017, 96302, and 116259) prior to now did not have a published self-consistent spectroscopic/astrometric joint orbital solution.

The paper is organized as follows: in Section 2, we present our list of SB1s, together with basic information relevant for our study; in Section 3, we present the results of our orbital calculations and mass ratios, and in Section 4, we present a detailed discussion of each of our objects. Finally, in Section 5, we present the main conclusions of our study.

2. The SB1 Sample

To select the sample for the present work, we started by doing a crossmatch between the Sixth Catalog of Orbits of Visual Binary Stars (Orb6) maintained by the US Naval Observatory[8] and SB9.

Orb6 is the most comprehensive catalog of binary systems with published orbital elements, while SB9 contains RV amplitudes for all binary systems for which it has been possible to fit a RV curve. Having identified those systems confirmed as SB1s in SB9, we pinpointed the binaries for which a combined astrometric/RV study of the orbit was not available in the literature, by means of the notes and comments given in Orb6 and SB9, and those that merited further study given new available data. This led to an initial working list of 36 binary systems.

For the systems selected as indicated above, we retrieved their RV data from SB9, or from references provided therein, and the astrometric data from the US Naval Observatory Fourth Catalog of Interferometric Measurements of Binary Stars[9] and from historical astrometry included in the Washington Double Star (WDS) Catalog effort (Mason et al. 2001; kindly provided to us by Dr. Brian Mason from the US Naval Observatory).

Finally, we included recent results obtained with the HRCam Speckle camera on the SOAR 4.1 m telescope at Cerro Pachón,[10] as part of our monitoring of southern binaries described in Mendez et al. (2017). We note that some of these measurements were secured after the publication of their last orbit, which allows for the improvement of the orbital solutions. We have also supplemented the published RVs with our own recent observations secured with the FEROS Echelle (Kaufer et al. 1999) high-resolution spectrograph on the 2.2 m MPG telescope[11] and the FIDEOS Echelle (Vanzi et al. 2018) on the 1 m telescope,[12] both operating at the ESO/La Silla Observatory, Chile. FEROS and FIDEOS spectra were reduced using the CERES pipeline (Brahm et al. 2017). In a couple of cases, we also found high-precision RV archival data for our binaries obtained during the planet-monitoring program being carried out with HARPS (Mayor et al. 2003) on the 3.6 m telescope at ESO/La Silla.[13] This added valuable and highly precise points to the RV curve.

Examination of the information collected showed that only 34 of the systems in our starting list had sufficient data to warrant further analysis. From this final working list, 12 SB1 systems were presented and studied in Videla et al. (2022), while the remaining 22 are included in the present paper. We must emphasize that, as a result of our selection process, our final sample is very heterogeneous and it should not be considered complete or representative of SB1 systems in any astrophysical sense. From this point of view, the main contribution of this paper is the addition of new orbits and mass ratios for these types of binaries, nine of which do not have a published joint estimation of their orbital parameters (to the best of our knowledge, ours is therefore the first combined orbit).

Table 1 presents the basic properties available in the literature for the sample studied in this work. The first two columns present the Hipparcos number and the discovery designation code assigned in the WDS Catalog. The following columns present the trigonometric parallax adopted as prior, the Reduced Unit Weight Error (RUWE—an indication of the reliability of the parallax) parameter as given in the Gaia catalog, the SpTy adopted for the primary component (from SIMBAD, Wenger et al. 2000, WDS, or our own estimate—as explained below), and the mass of the primary component implied by the SpTy.

The masses have been derived from the mass versus SpTy and mass versus luminosity class calibrations provided by Abushattal et al. (2020) or, if they are not available there, from Straizys & Kuriliene (1981). The dispersion in mass comes from assuming an SpTy uncertainty of $\pm$ one subtype, which is customary in spectral classification. As can be seen from this table, and as mentioned above, our SB1s represent a heterogeneous group of binaries, with masses in the range from $0.4M_{\odot}$ to slightly above $6M_{\odot}$, located at distances between 7 and 263 pc. Also, as we shall see in the following sections, the data quality and orbital phase coverage available for the sample is quite varied.

Regarding the trigonometric parallaxes used as priors, and indicated in the third column of Table 1, we note that for unresolved binary systems (separations smaller than about $0\farcs7$) and multiple systems, the Gaia solution can be compromised by acceleration and/or unresolved companions, because the current astrometric reductions assume single stars. The RUWE parameter given in the fourth column of this table highlights excessive astrometric noise, helping to identify suspicious astrometry (mainly those with RUWE >2.0; see, e.g., Tokovinin 2022). Accordingly, as can be seen in this table, most (but not all) of the systems studied here indeed have a high RUWE. This is an important issue that must be considered when analyzing the results for individual objects and the consistency between the different solutions.

To assign the SpTy to the primary components, listed in column five of Table 1, we consulted SIMBAD, the WDS catalog itself, and the Catalogue of Stellar Spectral Classifications by Skiff (2014), which provides a compilation of spectral classifications determined from spectral data alone (i.e., no narrowband photometry) and is updated regularly in VizieR

[8] Available at https://www.usno.navy.mil/USNO/astrometry/optical-IR-prod/wds/orb6.

[9] The latest version, called int4, is available at https://www.usno.navy.mil/USNO/astrometry/optical-IR-prod/wds/int4/fourth-catalog-of-interferometric-measurements-of-binary-stars.

[10] For up-to-date details of the instrument, see http://www.ctio.noao.edu/~atokovin/speckle/.

[11] See https://www.eso.org/sci/facilities/lasilla/instruments/feros.html.

[12] See https://www.eso.org/public/teles-instr/lasilla/1metre/fideos/.

[13] See https://www.eso.org/sci/facilities/lasilla/instruments/harps.html.

Table 1
Trigonometric Parallax, SpTy (Primary Component), and Mass (Primary Component) of the SB1 Stellar Systems Presented in This Paper

HIP #	Discovery Designation	ϖ[a] (mas)	RUWE[a]	SpTy[b] ($M_\odot$)	m_1[c]
3850	PES1	53.053 ± 0.028	0.9325	G9V[f]	0.93 ± 0.04
5336	WCK1Aa,Ab	130.29 ± 0.44	6.9658	G5V	1.05 ± 0.04
17491	BAG8AB	40.33 ± 0.25	11.5926	K0V	0.89 ± 0.04
28691	MCA24	3.82 ± 0.27	2.5179	B8III	3.44 ± 0.24
29860	CAT1Aa,Ab	51.62 ± 0.12	1.9793	F9V/G0V[f]	1.15 ± 0.04
36497	TOK392Da,Db	21.19 ± 0.18	5.8032	F8V	1.23 ± 0.05
38414	TOK195	8.98 ± 0.23	6.0362	K1/2II[f]	6.09 ± 0.07[g]
39261	MCA33	10.24 ± 0.22	5.8681	A2V/A3V[f]	2.27 ± 0.08
40167	HUT1Ca,Cb	40.89 ± 0.15	1.3840	F8V	1.23 ± 0.05
43109	SP1AB	26.437 ± 0.098	1.4190	G1III	1.02 ± 0.20
54061	BU1077AB	26.54 ± 0.48[d]	⋯	G9III	1.93 ± 0.26
55642	STF1536AB	41.93 ± 0.43[e,h]	⋯	F4IV	1.50 ± 0.05
67620	WSI77	53.88 ± 0.34[e]	⋯	G5V	1.05 ± 0.04
75695	JEF1	29.17 ± 0.76[d]	7.2964	A5V	1.54 ± 0.05
76031	TOK48	19.67 ± 0.89[d]	⋯	G0V	1.15 ± 0.04
78727	STF1998AB	35.89 ± 0.23	1.2934	F5IV	1.29 ± 0.05
93017	BU648AB	67.14 ± 0.12	2.7280	F9V/G0V[f]	1.20 ± 0.05
96302	WRH32	5.37 ± 0.10	1.5264	G8III	1.87 ± 0.26
103655	KUI103	66.554 ± 0.072	5.2017	M2V	0.43 ± 0.02
111685	HDS3211AB	51.2 ± 1.6[d]	31.988	M0V	0.54 ± 0.02
111974	HO296AB	29.59 ± 0.68[d]	⋯	G4V	1.06 ± 0.04
116259	HDS3356	29.23 ± 0.15	8.0906	G0V	1.15 ± 0.04

Notes. See the text for details.
[a] From GAIA DR3, except when noted.
[b] From SIMBAD, WDS, or from our own estimate—see the text for details.
[c] From Abushattal et al. (2020), except when noted.
[d] From HIPPARCOS.
[e] From GAIA DR2.
[f] Adopted the mean SpTy.
[g] From Straizys & Kuriliene (1981).
[h] Average of Gaia DR2 parallaxes for AB and C components.

(catalog B/mk/mktypes, currently containing more than 90,000 stars).

A comparison of the data from these three sources revealed that some objects in our sample have somewhat ambiguous SpTy. In order to resolve these ambiguities, we computed the absolute magnitude of the primary component, using the trigonometric parallax of the system listed in Table 1 and their apparent magnitudes given in the WDS catalog. This absolute magnitude was then compared with the absolute magnitude expected from the listed SpTy, using the calibrations provided by Abushattal et al. (2020). The SpTy closest to the computed absolute magnitude was finally adopted. We note that some ambiguities in the SpTy persisted after these calculations (see Section 4).

3. Orbital Elements and Mass Ratios

To determine the orbital parameters, we followed the scheme presented in detail in Videla et al. (2022). In summary, for each object, we are able to compute four orbital solutions, namely: one using no priors, as in classical works, denoted as the SB1 solution; one using the trigonometric parallax as a prior, denoted as the SB1 + $p(\varpi)$ solution; one using the mass of the primary as a prior, denoted as the SB1 + $p(m_1|\theta)$ solution; and, finally, a combined solution using parallax and mass as priors simultaneously, denoted as the SB1 + $p(\varpi)$ + $p(m_1|\theta)$ solution. These solutions are presented in Table 2. For reference, in the first two lines of each entry, we also present the orbital parameters given in Orb6 and SB9.

For each of our solutions, we provide the orbital elements obtained from the Maximum A Posteriori (MAP) estimation, which gives the most probable sample of the PDF, as well as the upper and lower values that encompass the 95% credible interval around the MAP solution (denoted as the High Posterior Density Interval, or HDPI, which encompasses the mode).

Of course, as explained in detail in Videla et al. (2022), only solutions that include a prior can lead to an estimation of the orbital parallax and the mass ratio, which are presented in the last columns of Table 2. We must note that the inferred parallaxes reported in this table cannot be properly called orbital parallaxes in the classical sense (as in the case of SB2 systems), because, while they have been derived self-consistently from the model and data, they are only resolvable by the incorporation of the priors. Nevertheless, throughout this paper, we will still refer to these as orbital parallaxes, to differentiate them from the trigonometric parallax adopted as prior. A plot of our MAP (pseudo) orbital parallaxes (from Table 2) versus the adopted prior parallax from Table 1 is shown in Figure 1, which exhibits a general good agreement between them, with a global rms of 0.97 mas over our 22 objects. In the right panel of Figure 1, the residuals have been normalized by the overall parallax uncertainty, which includes

Table 2

MAP Estimates and 95% HDPIs Derived from the Marginal PDFs of the Orbital Parameters for the Four Orbital Solutions, Based on Our Astrometric Data, Discussed in the First Paragraph of Section 3

HIP #	System	P (yr)	T (yr)	e	a (arcsec)	ω (°)	Ω (°)	i (°)	V_0 (km s^{-1})	ϖ (mas)	f/ϖ[a] (pc)	m_1 ($M_\odot$)	q
3850	Orb6	33.08 ± 0.70	1997.066 ± 0.0143	0.732 ± 0.0023	0.5199 ± 0.0512	266.90 ± 0.47	89.9 ± 1.4	46.3 ± 1.1	…	…	…	…	…
	SB9	31.74 ± 3.0626	2028.7857 ± 3.068	0.723 ± 0.013	…	-94.2 ± 1.6	…	…	9.93 ± *Fixed*	…	…	…	…
	SB1	$41.235^{48.786}_{36.471}$	$2032.630^{2035.724}_{2030.426}$	$0.456^{0.524}_{0.363}$	$0.426^{0.451}_{0.410}$	$331.331^{344.740}_{318.163}$	$17.371^{32.777}_{2.360}$	$4.529^{15.426}_{0.380}$	$10.325^{10.574}_{10.162}$	…	$24.804^{173.460}_{3.693}$	…	…
	SB1 + $p(\varpi)$	$31.754^{35.091}_{29.581}$	$2029.636^{2032.741}_{2027.474}$	$0.758^{0.774}_{0.737}$	$0.543^{0.624}_{0.483}$	$263.688^{267.484}_{262.780}$	$94.955^{103.084}_{84.513}$	$50.298^{58.591}_{43.456}$	$9.918^{9.962}_{9.880}$	$53.057^{53.106}_{52.999}$	$1.155^{1.327}_{1.001}$	$1.001^{1.251}_{0.777}$	$0.065^{0.076}_{0.056}$
	SB1 + $p(m_1\|\theta)$	$39.291^{49.103}_{36.457}$	$2031.769^{2035.702}_{2030.320}$	$0.480^{0.525}_{0.349}$	$0.421^{0.456}_{0.410}$	$326.008^{344.392}_{318.748}$	$22.870^{29.713}_{0.017}$	$7.705^{19.077}_{4.913}$	$10.262^{10.600}_{10.171}$	$31.556^{34.916}_{27.870}$	$12.609^{17.658}_{6.263}$	$0.926^{1.003}_{0.848}$	$0.661^{1.000}_{0.296}$
	SB1 + $p(\varpi)$ + $p(m_1\|\theta)$	$31.305^{32.926}_{29.895}$	$2029.210^{2030.483}_{2028.028}$	$0.753^{0.762}_{0.742}$	$0.528^{0.555}_{0.503}$	$263.981^{266.640}_{263.004}$	$93.501^{96.745}_{86.936}$	$48.460^{51.757}_{45.311}$	$9.926^{9.951}_{9.908}$	$53.059^{53.107}_{52.996}$	$1.189^{1.297}_{1.115}$	$0.941^{1.012}_{0.864}$	$0.067^{0.074}_{0.063}$
5336	Orb6	21.568 ± 0.015	1997.2235 ± 0.0067	0.5885 ± 0.0011	0.9985 ± 0.0013	330.37 ± 0.18	223.868 ± 0.064	110.671 ± 0.064	…	…	…	…	…
	SB9	21.4 ± 0.11	1975.901 ± 0.1	0.53 ± 0.02	…	150.0 ± 3.4	…	…	-97.35 ± 0.04	…	…	…	…
	SB1	$21.289^{21.317}_{21.250}$	$1997.358^{1997.434}_{1997.279}$	$0.558^{0.565}_{0.551}$	$1.029^{1.035}_{1.023}$	$151.763^{153.274}_{150.371}$	$45.581^{46.037}_{45.202}$	$107.723^{107.953}_{107.483}$	$-97.413^{-97.287}_{-97.526}$	…	$1.322^{1.436}_{1.233}$	…	…
	SB1 + $p(\varpi)$	$21.290^{21.319}_{21.251}$	$1997.360^{1997.433}_{1997.278}$	$0.558^{0.565}_{0.552}$	$1.028^{1.035}_{1.023}$	$151.854^{153.306}_{150.354}$	$45.604^{46.053}_{45.202}$	$107.723^{107.941}_{107.472}$	$-97.371^{-97.281}_{-97.519}$	$130.343^{131.162}_{129.468}$	$1.371^{1.445}_{1.246}$	$0.889^{0.927}_{0.868}$	$0.218^{0.232}_{0.193}$
	SB1 + $p(m_1\|\theta)$	$21.280^{21.316}_{21.251}$	$1997.347^{1997.429}_{1997.276}$	$0.558^{0.565}_{0.552}$	$1.029^{1.035}_{1.023}$	$151.683^{153.196}_{150.304}$	$45.599^{46.031}_{45.201}$	$107.745^{107.948}_{107.474}$	$-97.397^{-97.286}_{-97.520}$	$124.211^{127.363}_{121.247}$	$1.360^{1.444}_{1.239}$	$1.043^{1.123}_{0.966}$	$0.203^{0.218}_{0.182}$
	SB1 + $p(\varpi)$ + $p(m_1\|\theta)$	$21.282^{21.312}_{21.246}$	$1997.335^{1997.417}_{1997.261}$	$0.558^{0.565}_{0.551}$	$1.032^{1.037}_{1.025}$	$151.388^{152.982}_{150.040}$	$45.502^{45.973}_{45.125}$	$107.667^{107.889}_{107.411}$	$-97.454^{-97.301}_{-97.542}$	$130.034^{130.732}_{129.081}$	$1.271^{1.412}_{1.210}$	$0.921^{0.946}_{0.889}$	$0.198^{0.224}_{0.186}$
17491	Orb6	13.877 ± 0.016	1992.092 ± 0.016	0.2764 ± 0.003	0.2574 ± 0.0046	74.85 ± 0.25	281.1 ± 1.0	101.37 ± 0.12	…	…	…	…	…
	SB9	14.021 ± 0.123	1992.039 ± 0.070	0.275 ± 0.010	…	72.30 ± 2.16	…	…	22.238 ± 0.044	…	…	…	…
	SB1	$13.762^{13.897}_{13.658}$	$1992.017^{1992.111}_{1991.916}$	$0.263^{0.280}_{0.247}$	$0.254^{0.258}_{0.249}$	$72.003^{74.567}_{69.482}$	$281.083^{281.991}_{279.943}$	$101.987^{102.718}_{101.148}$	$22.312^{22.390}_{22.183}$	…	$10.330^{10.708}_{9.979}$	…	…
	SB1 + $p(\varpi)$	$13.767^{13.897}_{13.656}$	$1992.012^{1992.108}_{1991.910}$	$0.265^{0.281}_{0.248}$	$0.253^{0.258}_{0.249}$	$71.985^{74.497}_{69.425}$	$280.834^{281.952}_{279.916}$	$102.018^{102.723}_{101.168}$	$22.288^{22.384}_{22.175}$	$40.215^{40.800}_{39.819}$	$10.296^{10.750}_{10.019}$	$0.773^{0.827}_{0.698}$	$0.707^{0.764}_{0.672}$
	SB1 + $p(m_1\|\theta)$	$13.801^{13.897}_{13.653}$	$1992.020^{1992.113}_{1991.918}$	$0.264^{0.280}_{0.247}$	$0.253^{0.258}_{0.249}$	$72.409^{74.630}_{69.625}$	$281.113^{281.932}_{279.850}$	$101.778^{102.680}_{101.141}$	$22.306^{22.387}_{22.179}$	$38.620^{39.907}_{37.553}$	$10.395^{10.728}_{10.001}$	$0.884^{0.965}_{0.809}$	$0.671^{0.707}_{0.633}$
	SB1 + $p(\varpi)$ + $p(m_1\|\theta)$	$13.721^{13.879}_{13.638}$	$1992.035^{1992.126}_{1991.933}$	$0.274^{0.286}_{0.254}$	$0.257^{0.260}_{0.252}$	$72.234^{74.703}_{69.683}$	$280.936^{281.963}_{279.929}$	$101.624^{102.474}_{100.973}$	$22.267^{22.384}_{22.173}$	$40.081^{40.591}_{39.651}$	$10.117^{10.461}_{9.833}$	$0.828^{0.869}_{0.766}$	$0.682^{0.724}_{0.652}$
28691	Orb6	13.061 ± 0.03	2006.52 ± 0.16	0.808 ± 0.045	0.0555 ± 0.0022	291.5 ± 9.2	224.4 ± 3.3	111.8 ± 7.8	…	…	…	…	…
	SB9	12.98 ± 0.014	1980.807 ± 0.015	0.7407 ± 0.0042	…	125.30 ± 0.71	…	…	12.607 ± 0.052	…	…	…	…
	SB1	$13.012^{13.040}_{12.975}$	$1928.728^{1928.917}_{1928.590}$	$0.739^{0.747}_{0.730}$	$0.046^{0.048}_{0.044}$	$125.335^{126.837}_{124.013}$	$51.094^{55.451}_{47.951}$	$116.340^{122.285}_{110.006}$	$12.607^{12.710}_{12.491}$	…	$86.624^{94.033}_{79.458}$	…	…
	SB1 + $p(\varpi)$	$13.006^{13.040}_{12.977}$	$1928.760^{1928.906}_{1928.588}$	$0.737^{0.747}_{0.730}$	$0.046^{0.048}_{0.044}$	$125.758^{126.881}_{123.964}$	$52.315^{55.542}_{48.112}$	$116.431^{122.709}_{110.387}$	$12.580^{12.708}_{12.489}$	$3.867^{4.316}_{3.333}$	$86.960^{94.938}_{79.925}$	$6.543^{10.555}_{3.917}$	$0.507^{0.623}_{0.391}$
	SB1 + $p(m_1\|\theta)$	$13.009^{13.041}_{12.976}$	$1928.749^{1928.916}_{1928.593}$	$0.737^{0.747}_{0.730}$	$0.046^{0.048}_{0.044}$	$125.603^{126.919}_{124.043}$	$52.137^{55.530}_{48.022}$	$116.018^{122.700}_{110.283}$	$12.632^{12.708}_{12.491}$	$4.246^{5.528}_{3.853}$	$86.694^{94.788}_{79.729}$	$4.727^{5.790}_{1.497}$	$0.582^{0.901}_{0.493}$
	SB1 + $p(\varpi)$ + $p(m_1\|\theta)$	$13.013^{13.043}_{12.979}$	$1928.727^{1928.905}_{1928.584}$	$0.738^{0.748}_{0.730}$	$0.046^{0.047}_{0.044}$	$125.530^{126.928}_{124.055}$	$51.655^{54.833}_{47.300}$	$116.000^{123.755}_{111.186}$	$12.606^{12.706}_{12.487}$	$4.122^{4.433}_{3.756}$	$85.971^{96.688}_{81.065}$	$5.334^{6.887}_{3.785}$	$0.549^{0.665}_{0.477}$
29860	Orb6	35.52	1998.057	0.809	0.648	76.0	166.8	41.3	…	…	…	…	…
	SB9	34.20 ± 0.234	1998.050 ± 0.0013	0.8045 ± 0.0009	…	75.21 ± 0.15	…	…	−10.035 ± *Fixed*	…	…	…	…
	SB1	$43.460^{43.599}_{43.291}$	$1998.081^{1998.082}_{1998.080}$	$0.832^{0.833}_{0.832}$	$0.812^{0.816}_{0.805}$	$78.987^{79.100}_{78.865}$	$175.300^{175.519}_{174.989}$	$55.033^{55.359}_{54.595}$	$9.560^{9.564}_{9.555}$	…	$5.197^{5.258}_{5.150}$	…	…
	SB1 + $p(\varpi)$	$43.423^{43.590}_{43.284}$	$1998.081^{1998.082}_{1998.080}$	$0.832^{0.833}_{0.832}$	$0.810^{0.816}_{0.805}$	$78.957^{79.097}_{78.871}$	$175.284^{175.519}_{174.994}$	$54.944^{55.340}_{54.568}$	$9.558^{9.564}_{9.555}$	$51.674^{51.858}_{51.375}$	$5.209^{5.263}_{5.153}$	$1.492^{1.541}_{1.460}$	$0.368^{0.373}_{0.362}$
	SB1 + $p(m_1\|\theta)$	$43.430^{43.588}_{43.287}$	$1998.081^{1998.082}_{1998.080}$	$0.832^{0.833}_{0.832}$	$0.810^{0.816}_{0.805}$	$78.981^{79.101}_{78.870}$	$175.239^{175.514}_{175.004}$	$54.951^{55.359}_{54.619}$	$9.559^{9.564}_{9.555}$	$55.356^{56.245}_{54.733}$	$5.210^{5.256}_{5.150}$	$1.182^{1.222}_{1.124}$	$0.405^{0.414}_{0.399}$
	SB1 + $p(\varpi)$ + $p(m_1\|\theta)$	$43.337^{43.491}_{43.190}$	$1998.080^{1998.082}_{1998.079}$	$0.832^{0.832}_{0.832}$	$0.797^{0.802}_{0.792}$	$78.879^{79.008}_{78.778}$	$174.749^{174.962}_{174.475}$	$54.046^{54.367}_{53.674}$	$9.556^{9.561}_{9.552}$	$52.035^{52.285}_{51.843}$	$5.347^{5.399}_{5.299}$	$1.380^{1.407}_{1.349}$	$0.386^{0.391}_{0.381}$
36497	Orb6	7.621	2019.554	0.692	0.102	271.8	183.6	40.4	…	…	…	…	…
	SB9	7.415 ± 0.090	1981.605 ± 0.078	0.716 ± 0.098	…	263.19 ± 5.24	…	…	-2.379 ± 0.094	…	…	…	…
	SB1	$7.645^{7.675}_{7.607}$	$1981.398^{1981.495}_{1981.321}$	$0.643^{0.666}_{0.616}$	$0.093^{0.096}_{0.089}$	$265.146^{271.781}_{257.952}$	$192.723^{201.801}_{183.966}$	$32.491^{37.315}_{26.094}$	$-2.496^{-2.282}_{-2.648}$	…	$16.175^{20.638}_{13.290}$	…	…
	SB1 + $p(\varpi)$	$7.641^{7.675}_{7.604}$	$1981.406^{1981.497}_{1981.316}$	$0.642^{0.664}_{0.615}$	$0.092^{0.096}_{0.089}$	$264.965^{272.062}_{257.607}$	$192.611^{202.298}_{183.832}$	$31.683^{36.548}_{25.101}$	$-2.455^{-2.284}_{-2.658}$	$21.172^{21.531}_{20.827}$	$16.823^{21.304}_{13.633}$	$0.913^{1.113}_{0.666}$	$0.553^{0.812}_{0.398}$
	SB1 + $p(m_1\|\theta)$	$7.644^{7.677}_{7.607}$	$1981.408^{1981.495}_{1981.319}$	$0.639^{0.664}_{0.614}$	$0.092^{0.096}_{0.088}$	$264.960^{271.764}_{257.353}$	$192.895^{201.661}_{183.302}$	$30.794^{36.855}_{25.422}$	$-2.500^{-2.286}_{-2.659}$	$19.281^{20.734}_{18.047}$	$17.167^{21.408}_{13.716}$	$1.244^{1.324}_{1.131}$	$0.495^{0.641}_{0.395}$
	SB1 + $p(\varpi)$ + $p(m_1\|\theta)$	$7.632^{7.671}_{7.593}$	$1981.442^{1981.516}_{1981.358}$	$0.667^{0.684}_{0.649}$	$0.097^{0.099}_{0.095}$	$269.173^{274.364}_{263.164}$	$188.173^{196.820}_{179.813}$	$37.459^{39.810}_{34.716}$	$-2.426^{-2.258}_{-2.628}$	$21.123^{21.437}_{20.742}$	$13.386^{14.964}_{12.482}$	$1.200^{1.280}_{1.090}$	$0.394^{0.454}_{0.357}$
38414	Orb6	7.388 ± 0.657	2012.067 ± 0.206	0.380 ± 0.000	0.0624 ± 0.0071	170.0 ± 0.0	90.3 ± 6.8	86.2 ± 7.0	…	…	…	…	…
	SB9	6.9925	1905.51	0.38	…	170.	…	…	25.4	…	…	…	…
	SB1	$7.164^{7.224}_{7.114}$	$1984.310^{1984.537}_{1984.013}$	$0.553^{0.607}_{0.514}$	$0.055^{0.058}_{0.052}$	$204.818^{206.700}_{201.670}$	$89.931^{91.375}_{87.866}$	$75.422^{79.633}_{70.695}$	$7.337^{11.816}_{3.593}$	…	$185.367^{199.997}_{169.270}$	…	…
	SB1 + $p(\varpi)$	$7.586^{7.621}_{7.540}$	$1982.410^{1982.601}_{1982.273}$	$0.662^{0.724}_{0.625}$	$0.050^{0.052}_{0.047}$	$196.810^{201.030}_{192.150}$	$90.324^{92.329}_{88.135}$	$69.065^{74.513}_{61.549}$	$28.029^{29.008}_{26.712}$	$8.881^{9.413}_{8.520}$	$47.008^{57.014}_{41.607}$	$1.754^{1.995}_{1.212}$	$0.717^{1.000}_{0.615}$
	SB1 + $p(m_1\|\theta)$	$7.540^{7.606}_{7.441}$	$1982.637^{1983.057}_{1982.338}$	$0.672^{0.720}_{0.603}$	$0.050^{0.052}_{0.047}$	$198.631^{203.585}_{193.964}$	$89.770^{91.707}_{87.448}$	$68.068^{75.024}_{61.720}$	$26.403^{28.469}_{23.047}$	$6.011^{6.328}_{5.487}$	$64.513^{89.141}_{46.083}$	$6.058^{6.232}_{5.960}$	$0.633^{1.000}_{0.416}$
	SB1 + $p(\varpi)$ + $p(m_1\|\theta)$	$6.130^{6.161}_{6.097}$	$1981.852^{1982.007}_{1981.756}$	$0.497^{0.540}_{0.477}$	$0.058^{0.059}_{0.055}$	$157.473^{163.057}_{154.046}$	$95.118^{97.683}_{92.935}$	$79.683^{82.481}_{75.663}$	$26.411^{27.129}_{25.879}$	$8.464^{8.722}_{8.066}$	$33.337^{37.271}_{30.043}$	$6.058^{6.208}_{5.933}$	$0.393^{0.444}_{0.345}$
39261	Orb6	6.6504 ± 0.0089	2001.2281 ± 0.025	0.706 ± 0.024	0.055 ± 0.018	8.3 ± 1.8	118.3 ± 20.1	55.4 ± 2.9	…	…	…	…	…
	SB9	6.6312 ± 0.0066	1934.781 ± 0.0392	0.718 ± 0.012	…	5.22 ± 1.64	…	…	-2.10 ± 0.14	…	…	…	…
	SB1	$6.626^{6.646}_{6.598}$	$1981.187^{1981.205}_{1981.171}$	$0.777^{0.795}_{0.753}$	$0.052^{0.054}_{0.050}$	$13.176^{16.252}_{10.426}$	$113.564^{116.311}_{110.904}$	$47.889^{56.542}_{39.145}$	$-1.781^{-1.552}_{-2.026}$	…	$45.872^{53.677}_{38.446}$	…	…
	SB1 + $p(\varpi)$	$6.629^{6.648}_{6.601}$	$1981.189^{1981.204}_{1981.171}$	$0.777^{0.794}_{0.754}$	$0.053^{0.054}_{0.051}$	$13.929^{16.182}_{10.397}$	$113.970^{116.396}_{111.158}$	$51.126^{55.723}_{43.281}$	$-1.763^{-1.541}_{-2.022}$	$10.128^{10.643}_{9.799}$	$42.696^{49.059}_{39.686}$	$1.800^{2.041}_{1.355}$	$0.762^{0.999}_{0.699}$

Table 2
(Continued)

HIP #	System	P (yr)	T (yr)	e	a (arcsec)	ω (°)	Ω (°)	i (°)	V_0 (km s^{-1})	ϖ (mas)	f/ϖ[a] (pc)	m_1 ($M_\odot$)	q
	SB1 + $p(m_1\|\theta)$	$6.627^{6.647}_{6.599}$	$1981.195^{1981.204}_{1981.170}$	$0.769^{0.795}_{0.752}$	$0.053^{0.054}_{0.050}$	$14.193^{15.980}_{10.157}$	$113.275^{116.235}_{110.844}$	$50.481^{55.789}_{39.031}$	$-1.721^{-1.552}_{-2.025}$	$9.534^{9.783}_{8.769}$	$42.654^{53.832}_{38.986}$	$2.300^{2.459}_{2.144}$	$0.685^{0.919}_{0.611}$
	SB1 + $p(\varpi)$ + $p(m_1\|\theta)$	$6.635^{6.651}_{6.603}$	$1981.192^{1981.210}_{1981.174}$	$0.767^{0.784}_{0.744}$	$0.054^{0.055}_{0.052}$	$14.515^{17.334}_{11.403}$	$114.370^{116.627}_{111.651}$	$53.433^{58.896}_{47.021}$	$-1.761^{-1.509}_{-1.983}$	$9.790^{10.126}_{9.500}$	$40.589^{44.553}_{36.887}$	$2.265^{2.398}_{2.097}$	$0.659^{0.750}_{0.580}$
40167	Orb6	17.263 ± 0.032	1997.743 ± 0.160	0.180 ± 0.013	0.3592 ± 0.0058	287.3 ± 3.6	81.0 ± 1.9	150.0	…	…	…	…	…
	SB9	17.2539 ± 0.1615	1981.248 ± 0.3697	0.119 ± 0.018	…	307.0 ± 8.0	…	…	-7.93 ± 0.08	…	…	…	…
	SB1	$17.204^{17.220}_{17.185}$	$1983.188^{1983.357}_{1983.074}$	$0.103^{0.107}_{0.099}$	$0.379^{0.381}_{0.377}$	$343.309^{346.585}_{341.375}$	$68.351^{69.318}_{67.230}$	$143.574^{144.206}_{142.781}$	$-7.956^{-7.812}_{-8.039}$	…	$10.940^{11.377}_{10.398}$	…	…
	SB1 + $p(\varpi)$	$17.198^{17.220}_{17.185}$	$1983.212^{1983.357}_{1983.068}$	$0.103^{0.107}_{0.100}$	$0.379^{0.381}_{0.377}$	$343.552^{346.498}_{341.213}$	$68.340^{69.299}_{67.207}$	$143.455^{144.237}_{142.810}$	$-7.906^{-7.814}_{-8.036}$	$40.874^{41.163}_{40.598}$	$10.812^{11.395}_{10.422}$	$1.502^{1.568}_{1.412}$	$0.792^{0.869}_{0.739}$
	SB1 + $p(m_1\|\theta)$	$17.206^{17.219}_{17.185}$	$1983.247^{1983.358}_{1983.072}$	$0.104^{0.107}_{0.100}$	$0.380^{0.381}_{0.377}$	$344.352^{346.483}_{341.281}$	$67.951^{69.303}_{67.171}$	$143.282^{144.251}_{142.816}$	$-7.930^{-7.812}_{-8.030}$	$42.992^{44.095}_{42.000}$	$10.845^{11.366}_{10.400}$	$1.241^{1.323}_{1.127}$	$0.873^{0.948}_{0.820}$
	SB1 + $p(\varpi)$ + $p(m_1\|\theta)$	$17.200^{17.219}_{17.185}$	$1983.159^{1983.308}_{1983.016}$	$0.101^{0.104}_{0.098}$	$0.377^{0.379}_{0.375}$	$342.733^{345.510}_{340.264}$	$68.620^{69.538}_{67.432}$	$144.097^{144.749}_{143.392}$	$-7.903^{-7.821}_{-8.040}$	$41.054^{41.332}_{40.802}$	$11.317^{11.859}_{11.012}$	$1.404^{1.455}_{1.334}$	$0.868^{0.949}_{0.827}$
43109	Orb6	15.0507 ± 0.0064	1991.247 ± 0.005	0.6558 ± 0.0018	0.2547 ± 0.0009	266.10 ± 0.27	107.99 ± 0.35	50.01 ± 0.27	…	…	…	…	…
	SB9	15.04	1915.93	0.61	…	86.8	…	…	36.4	…	…	…	…
	SB1	$15.073^{15.084}_{15.063}$	$1900.819^{1900.878}_{1900.742}$	$0.656^{0.661}_{0.651}$	$0.253^{0.255}_{0.250}$	$85.086^{85.742}_{84.537}$	$288.913^{289.668}_{287.911}$	$49.960^{50.614}_{49.281}$	$35.613^{35.745}_{35.454}$	…	$16.337^{16.904}_{15.848}$	…	…
	SB1 + $p(\varpi)$	$15.072^{15.085}_{15.064}$	$1900.823^{1900.879}_{1900.740}$	$0.655^{0.661}_{0.651}$	$0.252^{0.255}_{0.250}$	$85.234^{85.742}_{84.593}$	$288.685^{289.637}_{287.984}$	$49.844^{50.538}_{49.242}$	$35.567^{35.739}_{35.450}$	$26.418^{26.637}_{26.245}$	$16.480^{16.901}_{15.849}$	$2.166^{2.300}_{2.053}$	$0.771^{0.810}_{0.721}$
	SB1 + $p(m_1\|\theta)$	$15.076^{15.084}_{15.063}$	$1900.801^{1900.889}_{1900.749}$	$0.657^{0.662}_{0.651}$	$0.253^{0.255}_{0.250}$	$85.158^{85.693}_{84.492}$	$288.851^{289.763}_{288.036}$	$50.005^{50.710}_{49.400}$	$35.633^{35.778}_{35.492}$	$30.191^{31.468}_{28.975}$	$16.289^{16.769}_{15.738}$	$1.315^{1.500}_{1.155}$	$0.968^{1.000}_{0.913}$
	SB1 + $p(\varpi)$ + $p(m_1\|\theta)$	$15.074^{15.087}_{15.066}$	$1900.812^{1900.867}_{1900.732}$	$0.654^{0.658}_{0.648}$	$0.252^{0.253}_{0.249}$	$85.265^{85.760}_{84.577}$	$288.568^{289.542}_{287.856}$	$49.655^{50.112}_{48.838}$	$35.526^{35.674}_{35.390}$	$26.535^{26.707}_{26.318}$	$16.667^{17.253}_{16.236}$	$2.094^{2.188}_{1.965}$	$0.793^{0.845}_{0.755}$
54061	Orb6	44.448 ± 0.11	2002.170 ± 0.094	0.4392 ± 0.004	0.590 ± 0.026	232.8 ± 7.9	9.3 ± 8.2	159.9 ± 3.5	…	…	…	…	…
	SB9	43.9992	1909.90	0.35	…	174.	…	…	−8.7	…	…	…	…
	SB1	$44.088^{44.452}_{43.914}$	$1914.123^{1914.496}_{1913.418}$	$0.433^{0.437}_{0.430}$	$0.594^{0.598}_{0.592}$	$53.716^{61.244}_{43.766}$	$187.957^{195.301}_{178.369}$	$165.364^{168.578}_{163.889}$	$-9.710^{-9.449}_{-9.964}$	…	$12.895^{18.327}_{8.960}$	…	…
	SB1 + $p(\varpi)$	$44.170^{44.447}_{43.912}$	$1913.957^{1914.492}_{1913.418}$	$0.433^{0.437}_{0.430}$	$0.595^{0.598}_{0.592}$	$52.500^{61.605}_{44.253}$	$186.795^{195.392}_{178.573}$	$165.438^{168.434}_{163.851}$	$-9.715^{-9.455}_{-9.961}$	$26.666^{27.485}_{25.595}$	$12.193^{18.433}_{10.194}$	$3.837^{4.366}_{2.803}$	$0.482^{0.937}_{0.352}$
	SB1 + $p(m_1\|\theta)$	$44.132^{44.438}_{43.898}$	$1914.044^{1914.511}_{1913.429}$	$0.433^{0.437}_{0.429}$	$0.595^{0.598}_{0.592}$	$55.901^{61.426}_{43.903}$	$190.032^{195.216}_{178.211}$	$165.754^{168.185}_{163.889}$	$-9.781^{-9.449}_{-9.959}$	$31.916^{35.259}_{29.187}$	$12.929^{16.685}_{9.978}$	$1.952^{2.402}_{1.401}$	$0.703^{0.999}_{0.521}$
	SB1 + $p(\varpi)$ + $p(m_1\|\theta)$	$44.199^{44.477}_{43.946}$	$1913.888^{1914.400}_{1913.334}$	$0.433^{0.437}_{0.430}$	$0.593^{0.597}_{0.591}$	$51.525^{60.446}_{41.935}$	$185.901^{194.695}_{176.651}$	$167.155^{169.404}_{165.236}$	$-9.681^{-9.429}_{-9.951}$	$27.211^{28.234}_{26.620}$	$17.792^{18.731}_{16.002}$	$2.736^{2.966}_{2.431}$	$0.938^{1.000}_{0.801}$
55642	Orb6	184.4572 ± 1.3275	1948.3626 ± 0.2117	0.53689 ± 0.00459	1.91525 ± 0.01550	142.829 ± 0.878	54.376 ± 0.846	127.642 ± 0.598	…	…	…	…	…
	SB9	191.996	1948.465	0.54	…	140.7	…	…	−11.0	…	…	…	…
	SB1	$189.516^{190.180}_{188.784}$	$1948.812^{1949.039}_{1948.553}$	$0.551^{0.553}_{0.547}$	$1.926^{1.937}_{1.919}$	$145.134^{145.836}_{144.501}$	$56.052^{56.616}_{55.712}$	$127.234^{127.504}_{126.787}$	$-11.151^{-11.108}_{-11.195}$	…	$10.523^{11.128}_{9.709}$	…	…
	SB1 + $p(\varpi)$	$189.419^{190.168}_{188.762}$	$1948.799^{1949.043}_{1948.553}$	$0.549^{0.553}_{0.547}$	$1.930^{1.937}_{1.918}$	$145.176^{145.864}_{144.537}$	$56.167^{56.606}_{55.709}$	$127.105^{127.501}_{126.791}$	$-11.142^{-11.111}_{-11.198}$	$41.726^{42.987}_{40.920}$	$10.263^{11.216}_{9.798}$	$1.576^{1.689}_{1.355}$	$0.749^{0.883}_{0.681}$
	SB1 + $p(m_1\|\theta)$	$189.317^{190.200}_{188.775}$	$1948.829^{1949.030}_{1948.554}$	$0.549^{0.553}_{0.547}$	$1.927^{1.937}_{1.919}$	$145.311^{145.822}_{144.527}$	$56.277^{56.608}_{55.714}$	$127.153^{127.489}_{126.809}$	$-11.150^{-11.109}_{-11.195}$	$43.111^{43.931}_{42.185}$	$10.348^{11.160}_{9.739}$	$1.379^{1.447}_{1.310}$	$0.805^{0.903}_{0.742}$
	SB1 + $p(\varpi)$ + $p(m_1\|\theta)$	$189.561^{190.192}_{188.747}$	$1948.860^{1949.053}_{1948.582}$	$0.550^{0.553}_{0.547}$	$1.926^{1.936}_{1.917}$	$145.345^{145.906}_{144.631}$	$56.178^{56.612}_{55.729}$	$127.249^{127.536}_{126.837}$	$-11.166^{-11.130}_{-11.207}$	$42.438^{43.259}_{41.949}$	$10.723^{11.360}_{10.113}$	$1.417^{1.461}_{1.336}$	$0.835^{0.921}_{0.768}$
67620	Orb6	10.485 ± 0.06	2009.218 ± 0.028	0.3462 ± 0.0080	0.2827 ± 0.0014	137.5 ± 1.4	171.3 ± 0.3	96.4 ± 0.2	…	…	…	…	…
	SB9	10.4786 ± 0.019	2009.248 ± 0.0329	0.3586 ± 0.0056	…	140.3 ± 1.3	…	…	5.242 ± 0.028	…	…	…	…
	SB1	$10.455^{10.470}_{10.441}$	$1998.842^{1998.879}_{1998.811}$	$0.340^{0.346}_{0.336}$	$0.286^{0.289}_{0.282}$	$141.958^{143.040}_{140.932}$	$171.617^{172.308}_{171.021}$	$96.031^{96.710}_{95.495}$	$5.351^{5.380}_{5.319}$	…	$7.175^{7.320}_{7.087}$	…	…
	SB1 + $p(\varpi)$	$10.456^{10.470}_{10.442}$	$1998.843^{1998.876}_{1998.806}$	$0.340^{0.346}_{0.336}$	$0.286^{0.288}_{0.282}$	$141.981^{143.062}_{140.945}$	$171.636^{172.369}_{171.040}$	$96.194^{96.724}_{95.511}$	$5.356^{5.381}_{5.321}$	$53.936^{54.546}_{53.196}$	$7.175^{7.315}_{7.090}$	$0.835^{0.882}_{0.776}$	$0.631^{0.656}_{0.614}$
	SB1 + $p(m_1\|\theta)$	$10.453^{10.470}_{10.442}$	$1998.850^{1998.877}_{1998.808}$	$0.340^{0.346}_{0.336}$	$0.285^{0.289}_{0.282}$	$142.167^{143.030}_{140.904}$	$171.738^{172.311}_{171.021}$	$96.250^{96.691}_{95.506}$	$5.348^{5.380}_{5.320}$	$50.662^{51.705}_{49.249}$	$7.182^{7.319}_{7.090}$	$1.037^{1.127}_{0.970}$	$0.572^{0.593}_{0.552}$
	SB1 + $p(\varpi)$ + $p(m_1\|\theta)$	$10.452^{10.466}_{10.437}$	$1998.842^{1998.875}_{1998.806}$	$0.339^{0.344}_{0.335}$	$0.289^{0.291}_{0.285}$	$141.761^{142.863}_{140.722}$	$171.539^{172.349}_{171.030}$	$96.138^{96.590}_{95.389}$	$5.361^{5.382}_{5.322}$	$53.095^{53.837}_{52.601}$	$7.093^{7.217}_{7.005}$	$0.917^{0.950}_{0.855}$	$0.604^{0.626}_{0.592}$
75695	Orb6	10.5367 ± 0.0014	1980.473 ± 0.0038	0.53971 ± 0.00021	0.204008 ± 0.000034	180.21 ± 0.13	148.041 ± 0.030	111.452 ± 0.014	…	…	…	…	…
	SB9	10.496	1938.197	0.41	…	185.4	…	…	−18.0	…	…	…	…
	SB1	$10.550^{10.553}_{10.546}$	$1906.630^{1906.669}_{1906.600}$	$0.524^{0.528}_{0.520}$	$0.207^{0.208}_{0.206}$	$180.651^{181.688}_{179.545}$	$148.315^{148.652}_{147.991}$	$110.874^{111.185}_{110.297}$	$-19.859^{-19.784}_{-19.924}$	…	$16.140^{16.385}_{15.891}$	…	…
	SB1 + $p(\varpi)$	$10.550^{10.553}_{10.546}$	$1906.632^{1906.669}_{1906.601}$	$0.524^{0.528}_{0.520}$	$0.207^{0.208}_{0.206}$	$180.739^{181.726}_{179.560}$	$148.340^{148.645}_{147.983}$	$110.668^{111.174}_{110.275}$	$-19.861^{-19.787}_{-19.929}$	$28.781^{30.648}_{27.769}$	$16.100^{16.380}_{15.879}$	$1.798^{2.032}_{1.380}$	$0.864^{0.984}_{0.809}$
	SB1 + $p(m_1\|\theta)$	$10.549^{10.553}_{10.546}$	$1906.636^{1906.669}_{1906.600}$	$0.524^{0.528}_{0.520}$	$0.207^{0.208}_{0.206}$	$180.604^{181.741}_{179.554}$	$148.313^{148.643}_{147.985}$	$110.763^{111.186}_{110.281}$	$-19.874^{-19.781}_{-19.927}$	$27.937^{28.455}_{27.520}$	$16.147^{16.373}_{15.878}$	$2.009^{2.122}_{1.885}$	$0.822^{0.852}_{0.796}$
	SB1 + $p(\varpi)$ + $p(m_1\|\theta)$	$10.549^{10.553}_{10.546}$	$1906.632^{1906.669}_{1906.601}$	$0.525^{0.528}_{0.520}$	$0.207^{0.208}_{0.206}$	$180.569^{181.784}_{179.606}$	$148.321^{148.646}_{147.980}$	$110.813^{111.141}_{110.257}$	$-19.856^{-19.787}_{-19.930}$	$28.066^{28.550}_{27.663}$	$16.103^{16.360}_{15.860}$	$1.982^{2.083}_{1.858}$	$0.825^{0.857}_{0.800}$
76031	Orb6	1.713 ± 0.002	2016.470 ± 0.010	0.435 ± 0.017	0.0427 ± 0.0010	45.8 ± 2.3	341.9 ± 2.1	150.0	…	…	…	…	…
	SB9	1.6956 ± 0.0038	2006.180 ± 0.0093	0.406 ± 0.014	…	43.2 ± 2.6	…	…	4.55 ± 0.09	…	…	…	…
	SB1	$1.697^{1.699}_{1.693}$	$2002.798^{2002.826}_{2002.783}$	$0.461^{0.484}_{0.432}$	$0.039^{0.040}_{0.037}$	$44.804^{51.325}_{40.852}$	$355.676^{360.000}_{352.768}$	$170.163^{176.872}_{161.733}$	$4.614^{4.908}_{4.287}$	…	$65.700^{190.218}_{29.739}$	…	…
	SB1 + $p(\varpi)$	$1.697^{1.700}_{1.693}$	$2002.810^{2002.832}_{2002.790}$	$0.457^{0.493}_{0.440}$	$0.041^{0.042}_{0.039}$	$48.314^{53.893}_{43.471}$	$356.260^{359.999}_{351.875}$	$153.961^{157.493}_{149.958}$	$4.672^{4.916}_{4.316}$	$19.262^{20.873}_{17.461}$	$24.282^{27.585}_{20.957}$	$1.727^{2.316}_{1.239}$	$0.879^{1.000}_{0.708}$
	SB1 + $p(m_1\|\theta)$	$1.696^{1.701}_{1.694}$	$2002.814^{2002.834}_{2002.790}$	$0.474^{0.498}_{0.445}$	$0.040^{0.042}_{0.039}$	$49.302^{54.297}_{43.654}$	$356.416^{360.000}_{351.466}$	$151.234^{153.730}_{148.193}$	$4.650^{4.939}_{4.321}$	$21.785^{23.088}_{20.739}$	$22.151^{23.900}_{19.831}$	$1.149^{1.238}_{1.082}$	$0.933^{1.000}_{0.834}$
	SB1 + $p(\varpi)$ + $p(m_1\|\theta)$	$1.698^{1.701}_{1.694}$	$2002.812^{2002.835}_{2002.790}$	$0.474^{0.498}_{0.445}$	$0.040^{0.041}_{0.038}$	$48.590^{54.227}_{43.531}$	$355.171^{359.998}_{351.179}$	$151.993^{154.062}_{149.757}$	$4.682^{4.931}_{4.313}$	$21.176^{22.100}_{20.337}$	$23.046^{24.422}_{21.487}$	$1.182^{1.249}_{1.101}$	$0.953^{1.000}_{0.884}$
78727	Orb6	45.90 ± 0.60	1997.22 ± 0.02	0.744 ± 0.001	0.654 ± 0.006	163.8 ± 5.0	25.3 ± 4.0	34.5 ± 1.0	…	…	…	…	…

Table 2
(Continued)

HIP #	System	P (yr)	T (yr)	e	a (arcsec)	ω (°)	Ω (°)	i (°)	V_0 (km s^{-1})	ϖ (mas)	f/ϖ[a] (pc)	m_1 ($M_\odot$)	q
	SB9	44.699	1905.39	0.75	⋯	343.6	⋯	⋯	−29.4	⋯	⋯	⋯	⋯
	SB1	$45.846^{45.909}_{45.817}$	$1859.564^{1859.646}_{1859.365}$	$0.746^{0.748}_{0.745}$	$0.666^{0.668}_{0.665}$	$155.300^{155.971}_{154.465}$	$32.841^{33.587}_{32.270}$	$34.607^{34.955}_{34.227}$	$-32.625^{-31.509}_{-34.038}$	⋯	$5.750^{9.470}_{1.274}$	⋯	⋯
	SB1 + $p(\varpi)$	$45.878^{45.911}_{45.819}$	$1859.467^{1859.648}_{1859.371}$	$0.747^{0.748}_{0.745}$	$0.667^{0.668}_{0.665}$	$155.171^{156.046}_{154.472}$	$32.937^{33.569}_{32.208}$	$34.648^{34.971}_{34.225}$	$-32.608^{-31.259}_{-33.717}$	$35.847^{36.492}_{35.251}$	$5.957^{10.687}_{2.811}$	$2.405^{2.774}_{1.881}$	$0.272^{0.577}_{0.087}$
	SB1 + $p(m_1\|\theta)$	$45.863^{45.911}_{45.818}$	$1859.515^{1859.660}_{1859.378}$	$0.746^{0.748}_{0.745}$	$0.667^{0.668}_{0.665}$	$155.219^{155.973}_{154.435}$	$32.899^{33.600}_{32.251}$	$34.631^{34.972}_{34.229}$	$-32.589^{-31.285}_{-33.775}$	$43.083^{45.295}_{39.385}$	$5.593^{10.350}_{2.347}$	$1.337^{1.398}_{1.303}$	$0.317^{0.680}_{0.109}$
	SB1 + $p(\varpi)$ + $p(m_1\|\theta)$	$45.855^{45.913}_{45.822}$	$1859.543^{1859.638}_{1859.361}$	$0.746^{0.748}_{0.745}$	$0.666^{0.668}_{0.665}$	$155.376^{156.028}_{154.496}$	$32.806^{33.528}_{32.201}$	$34.515^{34.901}_{34.145}$	$-30.595^{-30.139}_{-31.813}$	$36.960^{37.357}_{36.598}$	$13.424^{13.655}_{13.095}$	$1.404^{1.446}_{1.363}$	$0.985^{1.000}_{0.950}$
93017	Orb6	63.2489 ± 3.0169	1972.7274 ± 1.0996	0.21805 ± 0.05240	1.24739 ± 0.01764	288.164 ± 9.910	49.397 ± 0.773	115.743 ± 1.814	⋯	⋯	⋯	⋯	⋯
	SB9	$61.391 \pm$ *Fixed*	1972.220	0.25	⋯	102	⋯	⋯	-45.82 ± 0.69	⋯	⋯	⋯	⋯
	SB1	$61.285^{61.447}_{61.136}$	$1910.765^{1910.916}_{1910.601}$	$0.269^{0.273}_{0.266}$	$1.272^{1.275}_{1.270}$	$101.048^{101.432}_{100.639}$	$48.879^{49.040}_{48.659}$	$114.107^{114.237}_{113.980}$	$-45.947^{-45.857}_{-46.060}$	⋯	$5.825^{6.071}_{5.503}$	⋯	⋯
	SB1 + $p(\varpi)$	$61.291^{61.441}_{61.135}$	$1910.759^{1910.914}_{1910.608}$	$0.269^{0.273}_{0.266}$	$1.272^{1.275}_{1.270}$	$101.036^{101.433}_{100.642}$	$48.850^{49.045}_{48.672}$	$114.136^{114.241}_{113.987}$	$-45.961^{-45.858}_{-46.060}$	$67.125^{67.375}_{66.917}$	$5.785^{6.082}_{5.494}$	$1.108^{1.148}_{1.067}$	$0.635^{0.690}_{0.584}$
	SB1 + $p(m_1\|\theta)$	$61.274^{61.441}_{61.140}$	$1910.765^{1910.917}_{1910.615}$	$0.269^{0.273}_{0.266}$	$1.273^{1.275}_{1.270}$	$100.962^{101.452}_{100.667}$	$48.864^{49.032}_{48.658}$	$114.097^{114.243}_{113.985}$	$-45.942^{-45.860}_{-46.063}$	$65.963^{67.013}_{65.072}$	$5.812^{6.068}_{5.507}$	$1.180^{1.223}_{1.125}$	$0.622^{0.661}_{0.577}$
	SB1 + $p(\varpi)$ + $p(m_1\|\theta)$	$61.286^{61.417}_{61.117}$	$1910.743^{1910.932}_{1910.629}$	$0.270^{0.273}_{0.267}$	$1.273^{1.275}_{1.270}$	$100.938^{101.362}_{100.585}$	$48.839^{49.045}_{48.673}$	$114.072^{114.218}_{113.965}$	$-45.969^{-45.891}_{-46.082}$	$67.049^{67.301}_{66.859}$	$5.609^{5.852}_{5.384}$	$1.138^{1.166}_{1.104}$	$0.603^{0.648}_{0.567}$
96302	Orb6	4.56	1985.56	0.82	0.030	45.5	29.3	114.6	⋯	⋯	⋯	⋯	⋯
	SB9	4.303 ± 0.0011	1988.771 ± 0.0011	0.7787 ± 0.0018	⋯	139.6 ± 0.4	⋯	⋯	-17.26 ± 0.05	⋯	⋯	⋯	⋯
	SB1	$4.303^{4.306}_{4.301}$	$1919.920^{1919.953}_{1919.873}$	$0.789^{0.794}_{0.784}$	$0.029^{0.031}_{0.026}$	$139.671^{140.614}_{138.660}$	$181.511^{188.989}_{168.698}$	$106.470^{123.167}_{96.584}$	$-17.242^{-17.093}_{-17.375}$	⋯	$72.573^{88.625}_{64.879}$	⋯	⋯
	SB1 + $p(\varpi)$	$4.304^{4.306}_{4.301}$	$1919.910^{1919.952}_{1919.870}$	$0.788^{0.793}_{0.783}$	$0.029^{0.031}_{0.026}$	$139.491^{140.652}_{138.758}$	$179.270^{188.189}_{168.968}$	$107.302^{122.827}_{97.853}$	$-17.272^{-17.085}_{-17.372}$	$5.380^{5.581}_{5.176}$	$71.053^{89.369}_{66.395}$	$5.389^{6.252}_{2.890}$	$0.619^{0.913}_{0.539}$
	SB1 + $p(m_1\|\theta)$	$4.304^{4.306}_{4.301}$	$1919.904^{1919.952}_{1919.870}$	$0.788^{0.793}_{0.784}$	$0.028^{0.031}_{0.027}$	$139.593^{140.623}_{138.722}$	$181.684^{190.523}_{174.361}$	$104.776^{113.757}_{95.343}$	$-17.266^{-17.095}_{-17.374}$	$6.691^{7.516}_{6.175}$	$72.257^{79.134}_{65.111}$	$2.155^{2.423}_{1.775}$	$0.936^{1.000}_{0.893}$
	SB1 + $p(\varpi)$ + $p(m_1\|\theta)$	$4.303^{4.307}_{4.301}$	$1919.922^{1919.952}_{1919.869}$	$0.789^{0.794}_{0.784}$	$0.025^{0.026}_{0.024}$	$140.029^{140.815}_{138.951}$	$173.956^{179.938}_{168.656}$	$116.725^{121.808}_{110.479}$	$-17.195^{-17.083}_{-17.368}$	$5.464^{5.684}_{5.307}$	$89.468^{93.464}_{84.767}$	$2.611^{2.908}_{2.270}$	$0.956^{1.000}_{0.902}$
103655	Orb6	28.90	2007.26	0.656	0.709	116.0	143.5	36.3	⋯	⋯	⋯	⋯	⋯
	SB9	29.51 ± 0.66	1976.88 ± 0.046	0.717776 ± 0.014	⋯	308.961 ± 3.3	⋯	⋯	-33.9674 ± 0.095	⋯	⋯	⋯	⋯
	SB1	$29.466^{29.590}_{29.380}$	$1947.812^{1947.976}_{1947.594}$	$0.610^{0.617}_{0.605}$	$0.674^{0.678}_{0.669}$	$326.055^{328.055}_{322.815}$	$110.038^{113.120}_{108.160}$	$33.590^{34.754}_{31.994}$	$-33.698^{-33.524}_{-33.828}$	⋯	$7.202^{7.688}_{6.729}$	⋯	⋯
	SB1 + $p(\varpi)$	$29.488^{29.580}_{29.379}$	$1947.777^{1947.983}_{1947.616}$	$0.612^{0.616}_{0.606}$	$0.673^{0.678}_{0.670}$	$325.884^{328.224}_{323.178}$	$110.249^{112.916}_{108.185}$	$33.621^{34.759}_{32.166}$	$-33.651^{-33.523}_{-33.805}$	$66.536^{66.692}_{66.411}$	$7.099^{7.514}_{6.825}$	$0.629^{0.661}_{0.590}$	$0.895^{1.000}_{0.833}$
	SB1 + $p(m_1\|\theta)$	$29.488^{29.566}_{29.368}$	$1947.764^{1947.971}_{1947.609}$	$0.611^{0.615}_{0.604}$	$0.676^{0.680}_{0.671}$	$325.655^{328.803}_{323.925}$	$110.264^{111.780}_{107.252}$	$34.273^{35.475}_{33.095}$	$-33.600^{-33.452}_{-33.712}$	$73.521^{75.893}_{71.734}$	$6.750^{6.939}_{6.475}$	$0.451^{0.484}_{0.413}$	$0.985^{1.000}_{0.942}$
	SB1 + $p(\varpi)$ + $p(m_1\|\theta)$	$29.557^{29.637}_{29.443}$	$1947.675^{1947.882}_{1947.528}$	$0.615^{0.619}_{0.609}$	$0.668^{0.672}_{0.664}$	$324.365^{327.348}_{322.440}$	$111.956^{113.634}_{109.037}$	$32.325^{33.379}_{31.251}$	$-33.687^{-33.566}_{-33.817}$	$66.642^{66.751}_{66.465}$	$7.464^{7.521}_{7.409}$	$0.580^{0.593}_{0.569}$	$0.990^{1.000}_{0.976}$
111685	Orb6	16.77 ± 0.15	1991.78 ± 0.08	0.256 ± 0.009	0.330 ± 0.003	118.7 ± 2.2	69.0 ± 1.0	55.9 ± 0.6	⋯	⋯	⋯	⋯	⋯
	SB9	16.912 ± 0.0712	2008.719 ± 0.0601	0.249 ± 0.007	⋯	300.1 ± 1.3	⋯	⋯	-58.378 ± 0.113	⋯	⋯	⋯	⋯
	SB1	$16.748^{16.886}_{16.674}$	$1991.514^{1991.621}_{1991.347}$	$0.241^{0.251}_{0.227}$	$0.344^{0.347}_{0.340}$	$295.215^{296.834}_{293.082}$	$66.478^{67.583}_{65.561}$	$59.045^{59.804}_{57.954}$	$-58.203^{-57.963}_{-58.410}$	⋯	$6.977^{7.564}_{6.399}$	⋯	⋯
	SB1 + $p(\varpi)$	$16.754^{16.878}_{16.674}$	$1991.493^{1991.609}_{1991.345}$	$0.240^{0.250}_{0.227}$	$0.344^{0.347}_{0.340}$	$295.062^{296.814}_{293.103}$	$66.412^{67.554}_{65.548}$	$58.929^{59.859}_{57.988}$	$-58.148^{-57.956}_{-58.397}$	$51.432^{54.390}_{48.147}$	$6.997^{7.584}_{6.425}$	$0.682^{0.851}_{0.537}$	$0.562^{0.656}_{0.474}$
	SB1 + $p(m_1\|\theta)$	$16.761^{16.883}_{16.672}$	$1991.508^{1991.613}_{1991.340}$	$0.239^{0.251}_{0.228}$	$0.344^{0.347}_{0.340}$	$295.131^{296.878}_{293.108}$	$66.662^{67.624}_{65.591}$	$58.889^{59.859}_{57.953}$	$-58.208^{-57.952}_{-58.400}$	$54.998^{56.327}_{53.385}$	$6.865^{7.567}_{6.440}$	$0.542^{0.577}_{0.500}$	$0.607^{0.692}_{0.554}$
	SB1 + $p(\varpi)$ + $p(m_1\|\theta)$	$16.802^{16.893}_{16.683}$	$1991.478^{1991.614}_{1991.341}$	$0.239^{0.250}_{0.227}$	$0.342^{0.347}_{0.339}$	$295.410^{297.093}_{293.294}$	$66.556^{67.586}_{65.562}$	$58.596^{59.668}_{57.835}$	$-58.182^{-57.952}_{-58.399}$	$54.019^{55.465}_{52.817}$	$7.137^{7.703}_{6.578}$	$0.552^{0.589}_{0.514}$	$0.627^{0.703}_{0.564}$
111974	Orb6	20.829 ± 0.0030	1983.537 ± 0.0033	0.73499 ± 0.00014	0.28798 ± 0.000049	22.31 ± 0.12	251.540 ± 0.076	139.861 ± 0.032	⋯	⋯	⋯	⋯	⋯
	SB9	20.930	1983.570	0.72	⋯	204.2	⋯	⋯	−10.5	⋯	⋯	⋯	⋯
	SB1	$20.837^{20.851}_{20.826}$	$1900.181^{1900.226}_{1900.120}$	$0.733^{0.735}_{0.730}$	$0.290^{0.291}_{0.289}$	$22.007^{22.963}_{21.149}$	$251.203^{252.024}_{250.509}$	$139.355^{139.937}_{138.720}$	$-12.191^{-11.989}_{-12.346}$	⋯	$17.916^{18.324}_{17.449}$	⋯	⋯
	SB1 + $p(\varpi)$	$20.837^{20.849}_{20.826}$	$1900.177^{1900.230}_{1900.127}$	$0.732^{0.735}_{0.730}$	$0.290^{0.291}_{0.289}$	$21.893^{22.886}_{21.073}$	$251.118^{251.873}_{250.383}$	$139.178^{139.707}_{138.544}$	$-12.062^{-11.923}_{-12.263}$	$27.986^{28.785}_{27.331}$	$17.604^{18.028}_{17.236}$	$1.300^{1.397}_{1.177}$	$0.971^{1.000}_{0.948}$
	SB1 + $p(m_1\|\theta)$	$20.838^{20.849}_{20.824}$	$1900.175^{1900.236}_{1900.132}$	$0.732^{0.735}_{0.730}$	$0.290^{0.291}_{0.289}$	$21.671^{22.656}_{20.866}$	$250.820^{251.640}_{250.197}$	$138.771^{139.523}_{138.385}$	$-12.006^{-11.801}_{-12.102}$	$28.876^{29.399}_{28.425}$	$17.254^{17.535}_{16.948}$	$1.175^{1.227}_{1.112}$	$0.993^{1.000}_{0.983}$
	SB1 + $p(\varpi)$ + $p(m_1\|\theta)$	$20.836^{20.848}_{20.824}$	$1900.186^{1900.235}_{1900.129}$	$0.732^{0.735}_{0.730}$	$0.290^{0.291}_{0.289}$	$21.812^{22.626}_{20.829}$	$250.946^{251.645}_{250.194}$	$138.945^{139.530}_{138.403}$	$-11.960^{-11.802}_{-12.088}$	$29.005^{29.433}_{28.509}$	$17.210^{17.494}_{16.927}$	$1.158^{1.213}_{1.106}$	$0.997^{1.000}_{0.983}$
116259	Orb6	15.70 ± 0.23	2005.49 ± 0.01	0.536 ± 0.007	0.220 ± 0.002	89.5 ± 0.8	141.5 ± 0.3	75.1 ± 0.4	⋯	⋯	⋯	⋯	⋯
	SB9	16.654 ± 0.354	1989.325 ± 0.058	0.521 ± 0.012	⋯	97.0 ± 2.7	⋯	⋯	-3.359 ± 0.098	⋯	⋯	⋯	⋯
	SB1	$16.352^{16.392}_{16.285}$	$1989.136^{1989.180}_{1989.102}$	$0.537^{0.549}_{0.525}$	$0.223^{0.226}_{0.220}$	$87.683^{88.255}_{87.072}$	$141.842^{142.544}_{141.103}$	$74.466^{75.045}_{73.904}$	$-3.309^{-3.224}_{-3.415}$	⋯	$12.972^{13.303}_{12.452}$	⋯	⋯
	SB1 + $p(\varpi)$	$16.340^{16.392}_{16.284}$	$1989.146^{1989.181}_{1989.102}$	$0.542^{0.550}_{0.525}$	$0.223^{0.226}_{0.220}$	$87.779^{88.251}_{87.037}$	$141.865^{142.521}_{141.064}$	$74.587^{75.035}_{73.901}$	$-3.330^{-3.225}_{-3.418}$	$29.154^{29.518}_{28.924}$	$12.848^{13.310}_{12.469}$	$1.051^{1.103}_{0.969}$	$0.599^{0.639}_{0.573}$
	SB1 + $p(m_1\|\theta)$	$16.359^{16.396}_{16.286}$	$1989.136^{1989.179}_{1989.099}$	$0.541^{0.549}_{0.525}$	$0.223^{0.226}_{0.220}$	$87.691^{88.212}_{87.057}$	$142.018^{142.594}_{141.109}$	$74.431^{75.068}_{73.935}$	$-3.298^{-3.221}_{-3.414}$	$28.528^{29.100}_{27.713}$	$12.903^{13.308}_{12.463}$	$1.132^{1.226}_{1.068}$	$0.583^{0.605}_{0.549}$
	SB1 + $p(\varpi)$ + $p(m_1\|\theta)$	$16.349^{16.394}_{16.286}$	$1989.145^{1989.179}_{1989.101}$	$0.543^{0.553}_{0.530}$	$0.225^{0.227}_{0.222}$	$87.745^{88.123}_{86.962}$	$141.788^{142.623}_{141.155}$	$74.775^{75.183}_{74.129}$	$-3.310^{-3.223}_{-3.409}$	$29.076^{29.382}_{28.828}$	$12.672^{13.094}_{12.331}$	$1.093^{1.139}_{1.033}$	$0.583^{0.614}_{0.559}$

Note. m_1 and ϖ are the priors used for the mass of the primary component and the trigonometric parallax, respectively. In the first two lines (of six entries) for each SB1 system, we report the values provided by Orb6 and SB9, preserving the significant figures included in those catalogs as an indication of their precision.

[a] The parameter f/ϖ, with units of pc, introduced in Videla et al. (2022), condenses the pair of parameters ϖ, q, since they are not determinable, due to the absence of radial velocities for the secondary component, as in the case of SB2 systems.

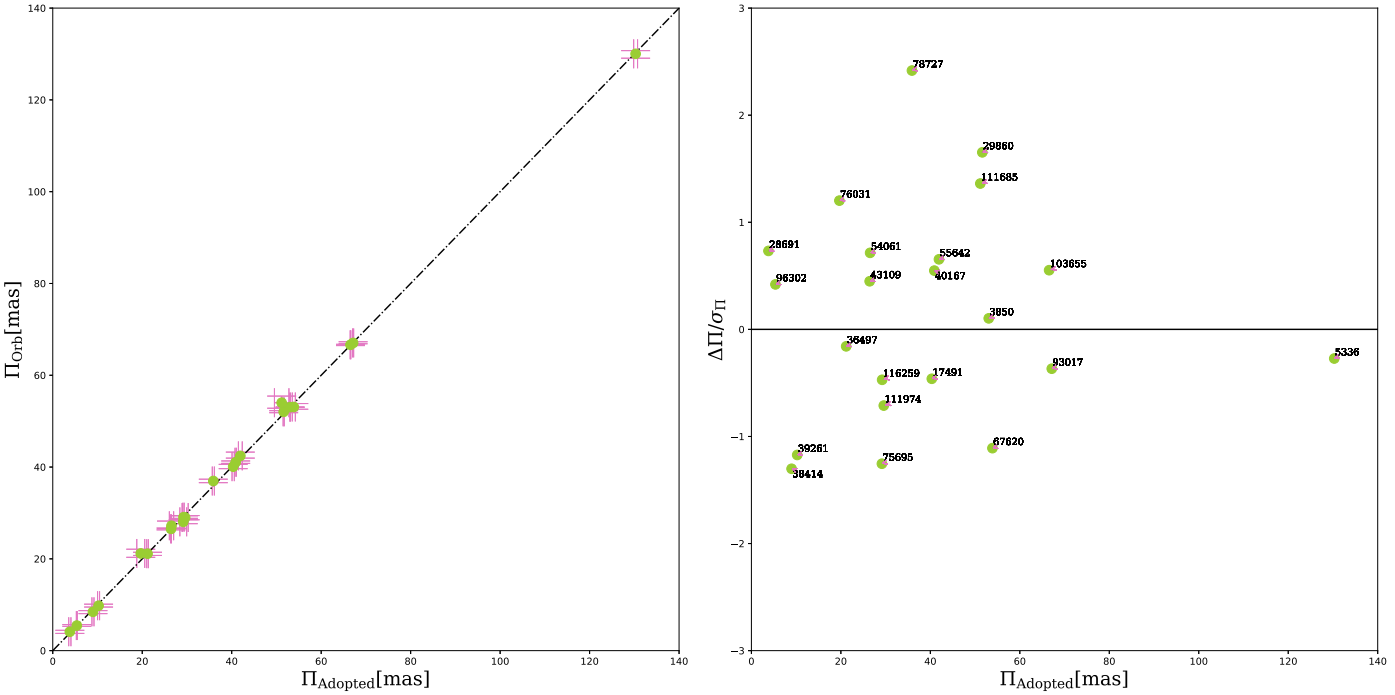

Figure 1. (Pseudo) orbital parallaxes from this work vs. the adopted prior parallax (left panel). In the right panel, we show the residuals in the sense $\Pi_{\rm Orb} - \Pi_{\rm Adopted}$ normalized by the parallax uncertainty of each target (see the text for details). The labels indicate the HIP numbers.

the uncertainty in the adopted parallax added in quadrature to the uncertainty of our estimated parallax.

A look at the results in Table 2 shows that our values for the orbital elements in general coincide quite well with those from previous studies. In particular, it is well known that periapsis (ω) can only be well determined by RV measurements as long as the distinction between primary and secondary is unambiguous (which is difficult, e.g., for equal-mass binaries); and the table shows our values are indeed quite close to those from SB9, but with smaller uncertainties in our case.[14]

On the other hand, the longitude of the ascending node (Ω) can be well determined from astrometric observations alone, but it is ambiguous in the case of equal-brightness binaries; and, additionally, it is subject to an ambiguity of $\pm 180°$, in which case the ω value is also affected by the same ambiguity (see Equation (28) in Appendix B.2 of Mendez et al. 2017).

This is clearly seen for HIP 28691: subtracting 180° from Ω and ω on Orb6 gives the SB9 and our values, while for HIP 43109 and HIP 54061, adding 180° to Ω and ω on Orb6 gives the SB9 and our values. Apart from these two cases, from the table we see that there is good correspondence between our values for Ω and those from Orb6 (but again with smaller formal uncertainties in our case, with a few exceptions). In terms of the other orbital elements, despite the fact that the sample is very heterogeneous, e.g., with periods ranging from 1.7 yr (HIP 76031) to 189 yr (HIP 55642) and with semimajor axes ranging from 25 mas (HIP 96302) to 1.″9 (HIP 55642), our solutions are, again, similar to those of previous studies, with the notable exception of HIP 29860, where a large difference is seen between our solution and previous studies. This case is further described below and in Figures 9 and 10. More specific notes and comments on individual objects are given below, in Section 4.

Figures 2–6 show the results for two representative SB1 systems studied here: HIP 38414 (TOK195) and HIP 43109 (SP1AB). The corresponding figures for all other SB1s presented in this paper can be found online at http://www.das.uchile.cl/~rmendez/B_Research/JAA_RAM_SB1/ and in Zenodo at doi:10.5281/zenodo.8269838.[15] In each case, we have produced graphical results of our simultaneous fits to the astrometric and RV data (for the SB1 + $p(\varpi)$ + $p(m_1|\theta)$ solution), corner plots, and PDFs for the orbital and physical parameters.

In Videla et al. (2022), a thorough experimental validation of the relative merits of each of the solutions was presented, depending on the prior used (see in particular Sections 3.1.4 and 3.2.4 of that paper). There, we conclude that the joint estimation of the orbit and RV curves, subject to the dynamical constraints of the Keplerian motion, allows the sharing of the knowledge provided by both sources of information (the trigonometric parallax and SpTy of the primary), reducing the uncertainty of the estimated orbital elements significantly, even if one source of information is highly noisy. Furthermore, we also show that the most robust estimate of the mass ratio is that obtained when both priors (SB1 + $p(\varpi)$ + $p(m_1|\theta)$) are used simultaneously. This is true even when there are relatively large differences in the solutions when using different priors, indicative that either the SpTy or the parallax may be somewhat in error or biased.

In Table 3, we present a global summary of our mass determination for primaries and secondaries based on the data on Table 2 and the respective tables in Videla et al. (2022; we adopt the combined solution using both priors, for the reasons

[14] Two notable cases where we maintain the ω value from Orb6, at odds with that reported from SB9, have indeed a $q \sim 1$, namely HIP 78727 and HIP 111974.

[15] In both locations, we also have the data used for our orbital solutions (astrometry and RVs) and their adopted errors. Our own Speckle observations are indicated as SOAR, while our RVs are indicated as FEROS or FIDEOS.

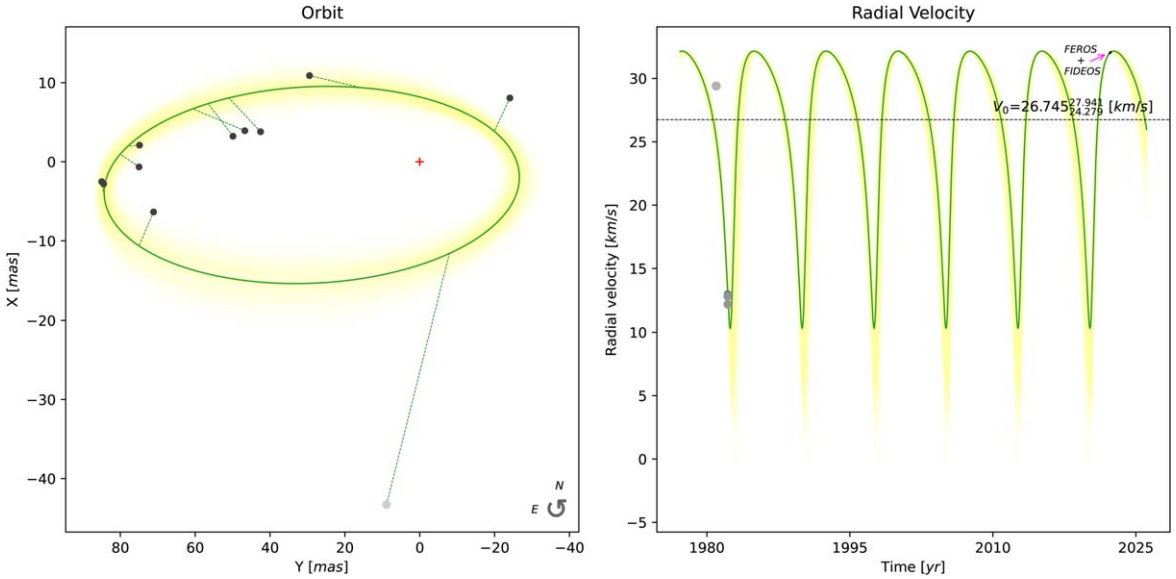

Figure 2. Orbit (left panel) and RV curve (right panel) for HIP 38414 based on the MAP values obtained from the SB1 + $p(\varpi)$ + $p(m_1|\theta)$ solution given in Table 2. The size and color of the dots in both plots depict the weight (uncertainty) of each observation: large clear dots indicate larger errors, and the opposite is true for small dark dots. In all astrometric orbits presented, smaller dots are from more recent interferometric measurements, including—but not limited to—our own (although in this particular case, all observations are from SOAR). For this system, we have a phase coverage of about 50% of the visual orbit. The large deviant point is from SOAR at 2011.9, so we gave it a smaller weight in our solution. For the RV curve, we supplemented good quality historical data with recent data acquired by us with FEROS and FIDEOS. The dashed horizontal line in the RV curve indicates the estimated systemic velocity, which is included, with its 95% HDPI range, at the right end of the line.

explained in the previous paragraph). In Table 3, the upper (m_2^+) and lower (m_2^-) masses for the secondary have been computed from $q^+ \cdot m_1^+$ and $q^- \cdot m_1^-$, respectively, where the + (or −) indicates the upper (lower) value of the respective quantities from Table 2 and its extension (in a way, this is the worst-case scenario for the range of predicted values).

3.1. A Pseudo Mass-to-luminosity Relationship from SB1s

As stressed in Videla et al. (2022), the scheme applied here to SB1 systems can only provide informed estimates of the mass ratio; definitive values for the individual masses of binary components can still only be obtained in the case of SB2 systems. It is interesting, however, to see how our inferred mass ratio values compare with a well-defined mass-to-luminosity relationship (MLR).

In Figure 7, a mass–luminosity plot, we show the positions of the 15 luminosity class V systems among our sample, superimposed to the mean fiducial lines given by Unwin et al. (2008; their Figures 5 and 6). In this plot, we have also included another eight luminosity class V systems, studied using the same methodology employed here, by Videla et al. (2022). The results included are those from the solution that provides the lowest uncertainty, which, as mentioned above, is the one that uses both priors (SpTy and the trigonometric parallax) simultaneously. As can be seen from this figure, there is an overall good agreement between the locations of the primaries and our inferred secondaries from the Bayesian statistical method employed here. We note that we do not pretend to build an MLR using these data; this exercise is meant to demonstrate that it is possible to derive tentative mass ratios for SB1 systems that could motivate further studies (e.g., attempting the detection/resolution of the secondary, given the q value and the implied luminosity).

As can be seen in Figure 7, the lateral dispersion (in mass) is reasonable. Indeed, the scatter on the mass of our derived secondary masses with respect to a fiducial line is small, amounting to 0.15 $M_\odot$ over the 22 secondaries plotted in Figure 7. The mass residuals are shown in Figure 8.

4. Discussion of Individual Objects

Based on Tokovinin's Multiple Star Catalog[16] (MSC; Tokovinin 1997, 2018), 12 of our studied binaries are actually in known multiple systems of different multiplicity; these are HIP 28691, 29860, 36497, 40167, 43109, 54061, 55642, 78727, 93017, 103655, 111685, and 111974. However, since we are looking at the inner (or tighter) components of these systems, their multiplicity does not seem to affect our results, based on an inspection of the residuals of our orbital solutions. The sole exception to this rule is HIP 78727, where we do see extant periodic residuals in position angle and separation, indicative of an unaccounted perturber.

HIP 3850 = PES1. This system has been extensively studied before by Peretti et al. (2019), using spectrophotometry and astrometry, and is a good comparison point for our methodology. The secondary is an L9-type benchmark brown dwarf, which leads to the lowest mass ratio q of our sample (the secondary is the point at the bottom right corner in Figure 7).

This system does not have interferometric data, but it has eight high-precision adaptive optics (AO) observations made with NACO at the ESO/Very Large Telescope at Cerro Paranal, Chile, covering slightly less than 10 yr of baseline. The orbital parameters have relatively large errors (especially the period, with a range from 28 to 34 yr), which is a consequence of the small number of observations and the restricted orbit coverage of the available astrometric data. We note that the value of $\omega = -94.^\circ2$ reported in SB9 is not inconsistent with our value of $+264.^\circ3$.

[16] An updated version is available at http://www.ctio.noirlab.edu/~atokovin/stars/.

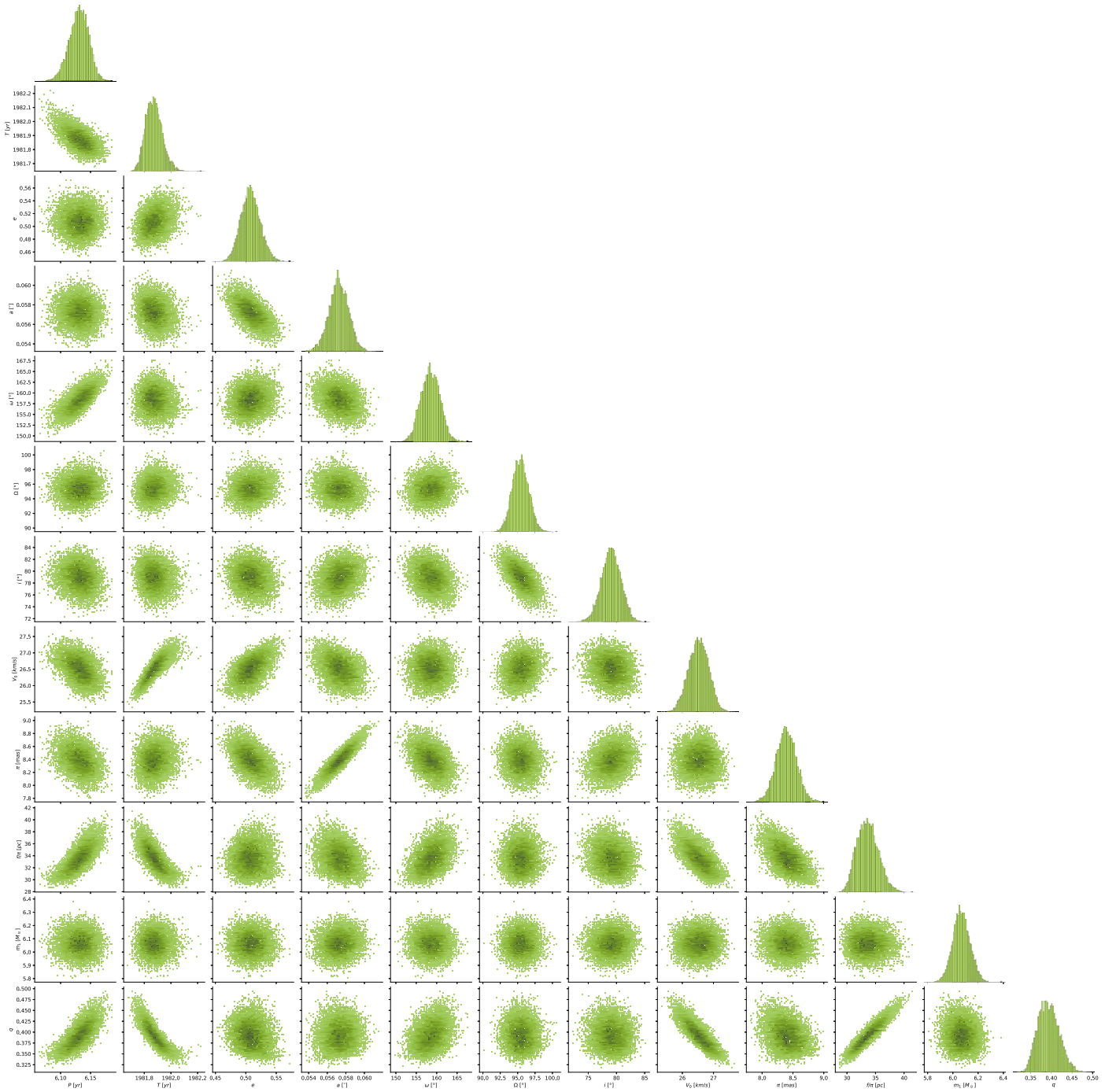

Figure 3. Corner plots for HIP 38414. These plots are useful for a qualitative assessment of the quality of the fit, in the sense that better-defined orbits, with enough phase coverage, have tight (usually Gaussian-like) PDFs, while less-defined orbits have rather disperse, tangled, and/or asymmetrical PDFs with long tails. Corner plots can also be used to uncover possible correlations between parameters that, if found to be systematic, can eventually be used to reduce the dimensionality of the inference. This is especially useful in problems of high dimensionality. In some cases, we have used these corner plots to check the consistency of our solutions when the SpTy is ambiguous (see the case of HIP 96302 in Section 4).

Precise RVs are available from observations made with CORALIE on the Swiss/ESO 1.3 m telescope at La Silla, Chile (Sahlmann et al. 2011), but they cover only 10.3 yr of the orbit. The SpTy published in WDS is G9V, and it is G8/K0V in SIMBAD, so we adopted G9V. It is interesting to note that Peretti et al. (2019) derive a primary mass of $0.856 \pm 0.014\,M_{\odot}$ and a secondary mass of $70.2 \pm 1.6\,M_{\rm Jup}$ from spectrophotometric data, giving a mass ratio of $q = 0.0783 \pm 0.022$, while our best solution (the last line of the first row of Table 2) gives an inferred value of $q = 0.067$, i.e., less than 1σ of their reported value. This gives strong support to the adequacy of our methodology. Although its semimajor axis is at the (lower) edge of the resolution of Gaia ($0\farcs53$), the large magnitude difference between primary and secondary (9.2 mag) leads to a small RUWE of 0.93, while the Hipparcos and Gaia parallaxes are equal within less than 1σ (considering the Hipparcos

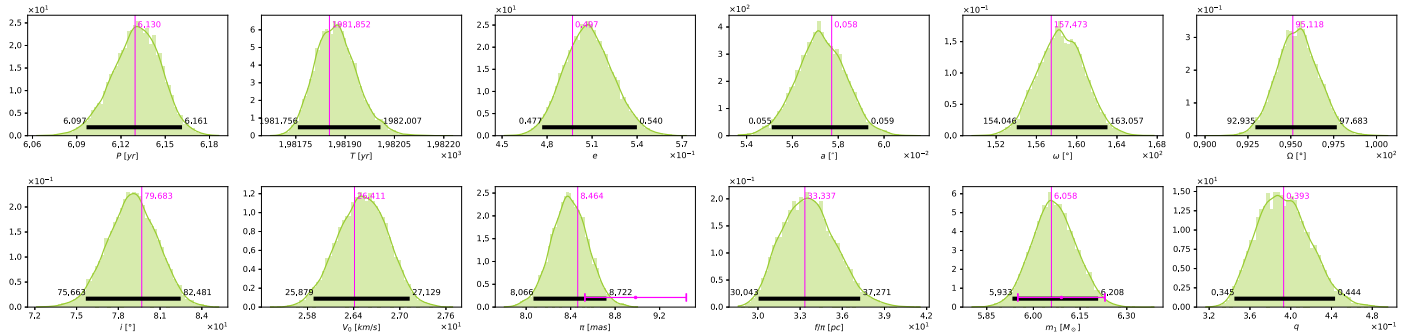

Figure 4. Marginal PDFs and MAP estimates (vertical magenta lines) for the orbital and physical parameters of the HIP 38414 binary system, for the SB1 + $p(\varpi)$ + $p(m_1|\theta)$ solution. The magenta horizontal error bars ($\pm 2\sigma$) indicate the priors adopted for ϖ and m_1, from Table 1.

uncertainty). Our systemic RV $V_0 = 9.926 \pm 0.025$ km s^{-1} compares well with the value reported by Gaia[17] of 9.71 ± 0.12 km s^{-1}.

HIP 5336 = WCK1Aa,Ab. This is the system with the second-lowest q. There are abundant historical and recent astrometric data covering most of the orbit (including high-resolution imaging secured with the Hubble Space Telescope, spanning almost two decades), as well as good-precision RV data. While SB9 indicates that a combined spectroscopic+visual solution has already been obtained by Agati et al. (2015), the authors do not list all the orbital elements of their orbit (see the second line of the second row of Table 2). On the contrary, our combined MCMC solution seems quite robust, with low formal uncertainties. Bond et al. (2020) have performed a more recent and detailed spectro-photometric and astrometric study of this system, obtaining $0.7440 \pm 0.0122\,M_\odot$ for the G5V primary and $0.1728 \pm 0.0035\,M_\odot$ for the dwarf-M companion, implying $q = 0.2335 \pm 0.0061$, which compares quite well with our inferred value of $q = 0.198 \pm 0.026$, considering our uncertainty. Our inferred mass for the primary ($0.921 \pm 0.032\,M_\odot$) is smaller than that expected for a G5V used as prior ($1.05 \pm 0.04\,M_\odot$; see Table 1 and the PDF on the web page), and it is more consistent with a G9V. Incidentally, the apparent magnitude for the primary from WDS and the parallax do imply an SpTy of G9/K0V. This object has a very large proper motion, $(\mu_\alpha \cos\delta, \mu_\delta) = (3468.25 \pm 0.35, -1564.94 \pm 0.37)$ mas, and a large negative systemic velocity, $V_0 = -97.5$ km s^{-1} (see the 10th column of Table 2), indicative of halo-like kinematics (the RV given by Gaia is -97.09 ± 0.25 km s^{-1}). Indeed, its measured metallicity indicates [Fe/H] ~ -0.75, the lowest measured value in our sample. Despite the large magnitude difference between primary and secondary (5.4 mag), it has a large RUWE (7.0). There is a large difference between the HIPPARCOS and Gaia parallaxes (more than 2 mas), probably because it is nearly resolved by Gaia (semimajor axis of 1.″0), being the nearest object in our sample, at 7.7 pc. There is a difference of 180° between the argument of periapsis (ω) and the longitude of the ascending node (Ω) as determined by us and the corresponding values obtained from the astrometry alone (from Orb6). This is a well-known ambiguity that can only be resolved by RV data.

HIP 17491 = BAG8AB. This object has a pretty good interferometric coverage of the orbit, except near periastron, and high-precision RV observations covering more than one period that were obtained with CORAVEL on the Danish/ESO 1.5 m telescope. As a prior for the SpTy, we adopted K0V, from SIMBAD, which is quite close to that given in WDS (G9.5V) and seemed more adequate given the (Gaia) parallax. There is, however, a rather large discrepancy between the HIPPARCOS and Gaia Data Release 3 (DR3) parallaxes (38.63 ± 0.79 versus 40.33 ± 0.25 mas, respectively). Our MAP parallax obtained from the combined solution is quite similar to that of Gaia (40.08 mas; see the 11th column and the last line of the third row in Table 2), despite the fact that the RUWE for this object is the second largest of our sample (see Table 1). This, in principle, indicates that the Gaia parallax could be biased, but it may be that the possible bias is being alleviated by the large brightness contrast: the primary has $V = 7.9$, while the secondary has $V = 10.7$, and hence the photocenter is almost coincident with the primary itself. A combined orbit is also reported by Balega et al. (2002), but it is not included in SB9 (only in Orb6), and hence no systemic velocity from this combined fit is available. Our value of 22.31 ± 0.13 km s^{-1} is not incompatible with Gaia at 26.44 ± 0.61 km s^{-1}, considering the amplitude of the velocity curve (see our web page with figures). Based on the Balega et al. (2002) study, Malkov et al. (2012) report $q = 0.723 \pm 0.074$, which is within 1σ of our value ($q = 0.682$).

HIP 28691 = MCA24. This is a triple system with an inner binary AaAb, but our analysis refers to the AB system alone (i.e., we used the center-of-mass velocity of the AaAb pair and the astrometry for AB). It is difficult to observe because the orbit is seen nearly edge-on and has a small semimajor axis ($a = 53$ mas) and a large eccentricity ($e = 0.74$). There are no data on the vicinity of periastron, and the astrometric data (including six recent data points, epochs 2015.9–2019.1 from our Speckle survey) cover only a small fraction of the orbit. This is compensated, in part, by abundant spectroscopic observations that cover several periods. In WDS, its SpTy is listed as B8III, but in SIMBAD, B8V is indicated. Based on the available photometry and trigonometric parallax, we find the primary to be more consistent with B8III and at a distance of about 262 pc (in agreement with the analysis by Fekel & Scarfe (1986). This is the most distant system and the second most massive of our sample. A combined spectroscopic/astrometric solution has already been obtained by Scarfe et al. (2000), but our new data add a handful of points that merit a revision of their solution.

[17] The RVs in the Gaia catalog result from the average over a variable time window (depending on the number of scans through the source), covering up to 34 months of observations (Katz et al. 2023).

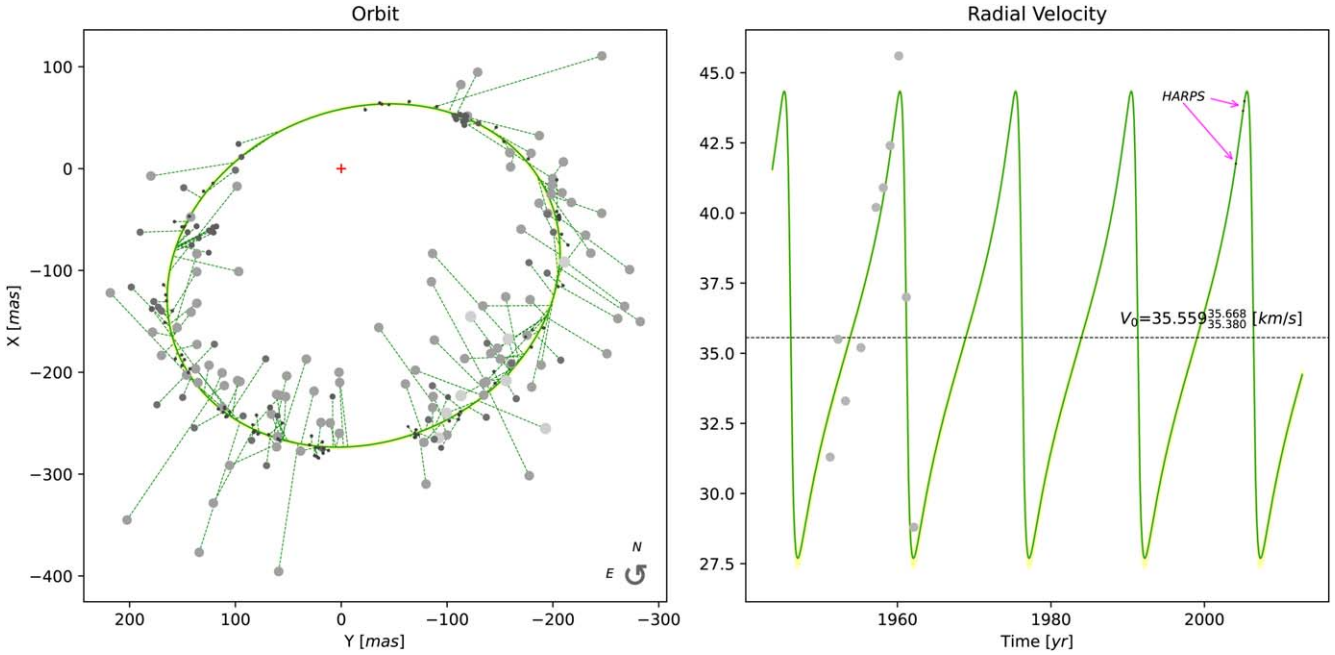

Figure 5. Similar to Figure 2, but for the HIP 43109 system. In this case, we have a good orbital coverage of the visual orbit (save for a small arc near periastron). The data points included are of different quality; some are historical RVs of decent quality and some are highly precise measurements at three consecutive epochs from HARPS at the ESO/La Silla 3.6 m telescope.

Independently, Tokovinin et al. (2020) published a purely astrometric orbit (listed in the Orb6 line of the corresponding entry in our Table 2). As can be seen from that table, our values for the combined solution, in particular for P and a, are both slightly smaller than those from Tokovinin et al. (2020) and with slightly larger errors; about halfway from the SB9 values (at least for P). Our MAP parallax is found to be 4.1 mas, close to the Gaia parallax of 3.8 mas, and within 1σ of their uncertainties. In contrast, the Hipparcos parallax for this system is reported to be 4.54 ± 0.29 mas, which is probably biased. The same correction on ω and Ω as for HIP 5336 is seen in this system (see Table 2).

HIP 29860 = CAT1Aa,Ab. This is the first fully combined orbit for the AaAb subsystem (WDS name CAT*1) of this apparently septuple system. It has the largest eccentricity ($e = 0.83$) of the objects in our sample. Less than half the orbit is covered, mostly by our own Speckle data secured between 2008 and 2020. Old, low-precision RV data have been supplemented with recent data from our FIDEOS and FEROS monitoring program (with formal uncertainties on the order of 0.01 km s^{-1}), which has greatly helped to pin down the period. Our first attempts to fit the orbit with our astrometric + RV data failed miserably, because the RVs published in SB9 were completely off scale. A careful look at the source of those RVs in Katoh et al. (2013) shows that some arbitrary zero-point offsets were applied to the old data to conform to their own data. These authors, however, were not concerned with the systemic velocity.[18] Specifically, in their Table 2, they indicate offsets of -5.2550 and -14.2000 km s^{-1} applied to the data from Vogt et al. (2002) and Beavers & Eitter (1986), respectively, in order for these data to conform to theirs. Because our data indicate that the RVs from Katoh et al. (2013) are completely off, we undid these corrections, applying offsets of $+14.2000$ km s^{-1} to the data from Katoh et al. (2013; effectively putting the RV scale on the zero-point of Beavers & Eitter 1986) and of $+8.945$ km s^{-1} to the data from Vogt et al. (2002), while not applying any offset to the data from Beavers & Eitter (1986). These were the historic RVs used for our fits, and they are available in the data tables on the web page[19] and in Zenodo.[20] The final combined fit to this system is shown in Figure 9, which shows the excellent correspondence between the (corrected) RVs from Vogt et al. (2002; epochs 1996 to 2001, near periastron) and Katoh et al. (2013; epochs 2006 to 2009) with our recent data points from FEROS and FIDEOS. In Figure 10, we show the corresponding PDFs. Our systemic velocity, 9.556 ± 0.005 km s^{-1}, agrees reasonably well with the Gaia value at 8.70 ± 0.20 km s^{-1} (certainly within the RV curve; see the right plot of Figure 9), giving us further confidence in our zero-point renormalization procedure.

In the notes of Orb6, it is indicated that the individual masses are $0.96 \pm 0.18\,M_\odot$ and $0.67 \pm 0.04\,M_\odot$ from Catala et al. (2006), derived from ground-based AO observations of the AaAb pair made with the Canada–France–Hawaii (CFH) telescope at Mauna Kea, plus the RVs from Vogt et al. (2002) alone. Note that the CFH observations cover a very short arc (3 yr), considering the orbital period (44 yr). They reported a period of 28.8 ± 1.1 yr, which is significantly smaller than all values published since then (see the Orb6 and SB9 values), including our own fitted value. Their semimajor axis is also smaller, $a = 0\farcs621 \pm 0\farcs019$. Our derived primary mass is somewhat larger, at $1.38 M_\odot$, leading to a smaller q (0.386 ± 0.005) than that implied by Catala et al. (2006; 0.491 ± 0.064), albeit within 1.6σ of their

[18] Indeed, in the notes to SB9, it says: "No systemic velocity provided in the paper, the value reported and the offset have been supplied by the author directly."

[19] http://www.das.uchile.cl/~rmendez/B_Research/JAA_RAM_SB1/

[20] doi:10.5281/zenodo.8269838

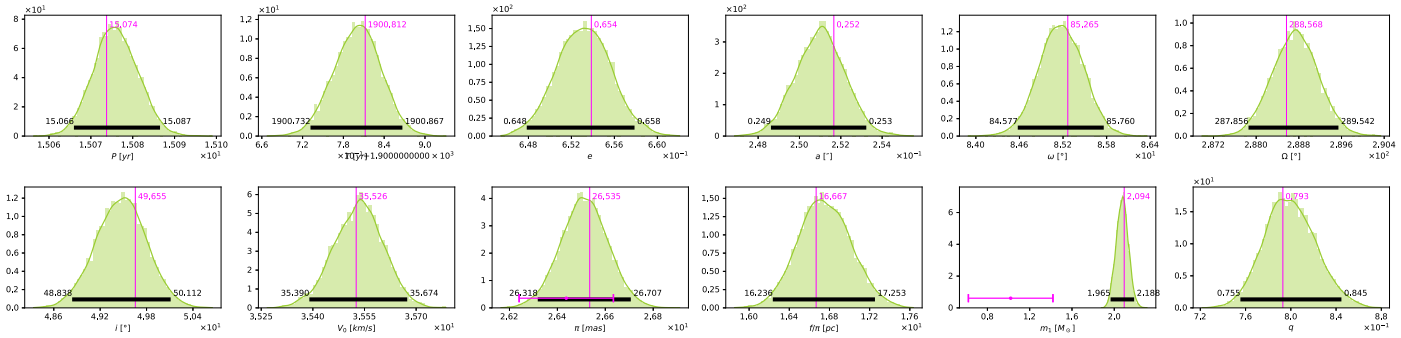

Figure 6. Similar to Figure 4, but for the HIP 43109 system.

Table 3
Estimated Mass of the Primary and Secondary Components of the SB1 Stellar Systems Presented in This Paper, and in Videla et al. (2022), Obtained when Both Priors (SB1 + $p(\varpi)$ + $p(m_1|\theta)$) are Used Simultaneously

HIP #	Discovery Designation	m_1 ($M_\odot$)	m_2 ($M_\odot$)
171	BU733AB	$0.927^{0.959}_{0.907}$	$0.721^{0.762}_{0.684}$
3504	NOI3Aa,Ab	$5.765^{7.726}_{3.812}$	$4.658^{7.726}_{2.695}$
3850	PES1	$0.941^{1.012}_{0.864}$	$0.063^{0.075}_{0.054}$
5336	WCK1Aa,Ab	$0.921^{0.946}_{0.889}$	$0.182^{0.212}_{0.165}$
6564	BU1163	$1.317^{1.396}_{1.225}$	$1.275^{1.396}_{1.134}$
7918	MCY2	$1.008^{1.035}_{0.981}$	$0.289^{0.302}_{0.279}$
17491	BAG8AB	$0.828^{0.869}_{0.766}$	$0.565^{0.629}_{0.499}$
28691	MCA24	$5.334^{6.887}_{3.785}$	$2.928^{4.580}_{1.805}$
29860	CAT1Aa,Ab	$1.380^{1.407}_{1.349}$	$0.533^{0.550}_{0.514}$
36497	TOK392Da,Db	$1.200^{1.280}_{1.090}$	$0.473^{0.581}_{0.389}$
38414	TOK195	$6.058^{6.208}_{5.933}$	$2.381^{2.756}_{2.047}$
39261	MCA33	$2.265^{2.398}_{2.097}$	$1.493^{1.799}_{1.216}$
40167	HUT1Ca,Cb	$1.404^{1.455}_{1.334}$	$1.219^{1.381}_{1.103}$
43109	SP1AB	$2.094^{2.188}_{1.965}$	$1.661^{1.849}_{1.484}$
54061	BU1077AB	$2.736^{2.966}_{2.431}$	$2.566^{2.966}_{1.947}$
55642	STF1536AB	$1.417^{1.461}_{1.336}$	$1.183^{1.346}_{1.026}$
65982	HDS1895	$0.920^{0.955}_{0.878}$	$0.581^{0.826}_{0.441}$
67620	WSI77	$0.917^{0.950}_{0.855}$	$0.554^{0.595}_{0.506}$
69962	HDS2016AB	$0.752^{0.814}_{0.700}$	$0.401^{0.483}_{0.337}$
75695	JEF1	$1.982^{2.083}_{1.858}$	$1.635^{1.785}_{1.486}$
76031	TOK48	$1.182^{1.249}_{1.101}$	$1.126^{1.249}_{0.973}$
78401	LAB3	$18.090^{29.606}_{8.753}$	$10.709^{22.797}_{3.965}$
78727	STF1998AB	$1.404^{1.446}_{1.363}$	$1.383^{1.446}_{1.295}$
79101	NOI2	$2.350^{2.661}_{2.147}$	$1.699^{2.661}_{1.168}$
81023	DSG7Aa,Ab	$1.019^{1.076}_{0.972}$	$1.013^{1.076}_{0.961}$
93017	BU648AB	$1.138^{1.166}_{1.104}$	$0.686^{0.756}_{0.626}$
96302	WRH32	$2.611^{2.908}_{2.270}$	$2.496^{2.908}_{2.048}$
99675	WRH33Aa,Ab	$9.440^{10.949}_{8.048}$	$6.476^{9.964}_{5.078}$
103655	KUI103	$0.580^{0.593}_{0.569}$	$0.574^{0.593}_{0.555}$
109951	HDS3158	$0.958^{0.990}_{0.934}$	$0.922^{0.990}_{0.802}$
111685	HDS3211AB	$0.552^{0.589}_{0.514}$	$0.346^{0.414}_{0.290}$
111974	HO296AB	$1.158^{1.213}_{1.106}$	$1.155^{1.213}_{1.087}$
115126	MCA74Aa,Ab	$1.195^{1.241}_{1.151}$	$0.754^{0.804}_{0.708}$
116259	HDS3356	$1.093^{1.139}_{1.033}$	$0.637^{0.699}_{0.577}$

inferred value and errors. We note that our PDFs indicate that the posterior mass for the primary actually tends to be slightly larger than the input a priori mass for an F9.5V ($1.15\,M_\odot$) from Abushattal et al. (2020), while the a priori and the posterior parallax are, within the errors, commensurable to each other (see Figure 10).

HIP 36497 = TOK392Da,Db. Ours is the first combined orbit for this SB1 binary, which is a member of a quadruple system. About one-half of the astrometric orbit of the pair is covered by our Speckle data. A previous attempt with the Robo-AO system failed to resolve the binary (Riddle et al. 2015). There are abundant high-quality RV data secured with CORAVEL, covering almost three full periods. There is no ambiguity in the SpTy (F8V). Despite its elevated RUWE (5.80), the Hipparcos, Gaia, and our own MAP parallaxes agree well. Once again, as was the case for HIP 17491, the primary has $V = 8.0$ mag, while the secondary has $V = 11.7$ mag, so the photocenter is almost coincident with the primary itself, which could explain the high RUWE. Our systemic velocity of -2.43 ± 0.20 km s^{-1} is compatible with the Gaia value at -2.07 ± 0.43 km s^{-1}.

HIP 38414 = TOK195. Ours is the first combined orbit for this relatively short-period SB1 system at about 110 pc from the Sun. The K1/2II red giant primary component is the most massive primary object ($6.1\,M_\odot$) of our sample. The few historic (from the 1980s) RV points taken from Parsons (1983) supplement our own RVs, derived from FEROS and FIDEOS observations secured in 2022, which greatly helped our joint solution. The astrometric data cover about one-half of the orbit and are all from our SOAR program. The somewhat elevated residuals are due to the small semimajor axis (62 mas) and the large inclination (almost 80°; see Figure 2).[21] While the RUWE value is large (6.0), the difference between the Hipparcos and Gaia parallaxes is small, less than 0.3 mas, within 1σ of the Gaia uncertainty. Our MAP orbital parallax is 8.46 ± 0.40 mas, 0.79 mas smaller than the Gaia parallax, but almost within 1σ, considering the Gaia error (see Figure 4). Finally, it is noteworthy that, given its parallax and photometry, the absolute magnitude ($M_V = -1.0$) is not consistent with a K1.5II star. According to Straižys & Kuriliene (1981), their Table 2, it is about $M_V = -2.5$. We have no explanation for this discrepancy.

HIP 39261 = MCA33. About one-half of the astrometric orbit has been covered for this object and there are abundant RV data of variable precision covering more than two revolutions. According to the notes of Orb6, the mass sum for this system reported in the literature spans a wide range; from $4.1\,M_\odot$ (Scholz & Lehmann 1988) or $3.61 \pm 0.38\,M_\odot$ (according to Balega et al. 2004) to $1.49 \pm 0.66\,M_\odot$ (from Carrier et al. 2002). Our inferred total mass of the system,

[21] Indeed, in the notes to Orb6, it says: "The binary is difficult to measure, always close to the diffraction limit (on a 4 m telescope), and with a magnitude difference ~3."

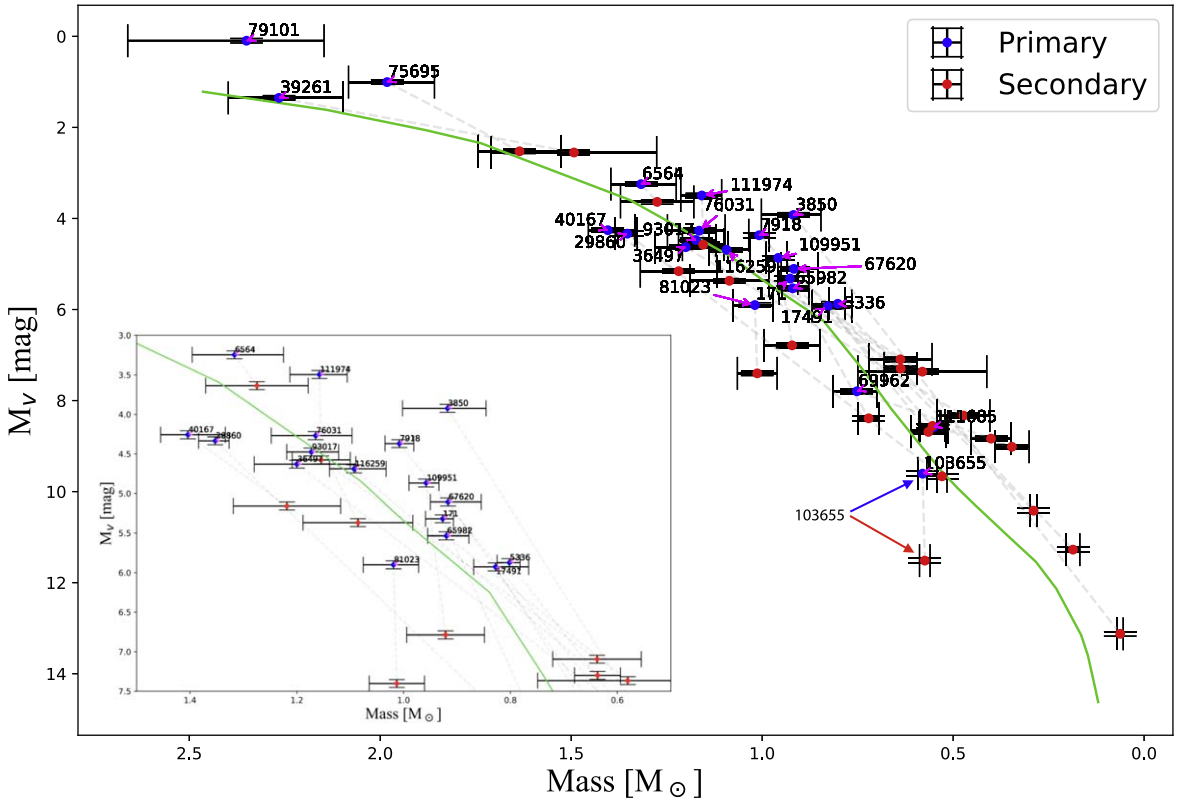

Figure 7. Pseudo MLR from the 23 SB1 systems of luminosity class V in our sample. The plot inserted shows a zoom-in on the mass range from 0.5 to 1.5 $M_\odot$, with M_V from +3.0 to +7.5. Primary components are depicted with a blue dot and secondaries with a red dot. The components of each binary are joined by a thin dashed line (the most massive object, HIP 7901, presented in Videla et al. 2022, does not have photometry for its secondary, hence only the primary star is shown here). The uncertainties on the mass of the primary and secondary are directly based on the values given in the last row of each entry in Table 2 (and the corresponding table in Videla et al. 2022), while we have assumed an uncertainty of ∼0.05 mag in M_V as a representative value, considering the errors in the photometry and distance.

based on the results of Table 2, is $3.73 \pm 0.32\,M_\odot$ and is within 1σ of the joint astrometric+spectroscopic solution of Balega et al. (2004). The PDF for the parallax indicates that our solution has a slightly smaller value than that of Gaia, but within 1.2σ, so our mass estimate does not seem to be affected by the small inferred parallax. The Hipparcos parallax, at 10.13 ± 0.52 mas, agrees well with Gaia (despite the elevated RUWE at 5.9) and with our MAP parallax.

HIP 40167 = HUT1Ca,Cb. Ours is the first combined orbit. This SB1 system is the CaCb subsystem of a septuple (and, possibly, octuple) system. The coverage of the orbit is good, the last 13 points being from our Speckle survey (2016.9–2021.0). The first astrometric measurement is from Hipparcos (1991.25). It also has abundant RV data of reasonable precision covering slightly more than one period. WDS reports an SpTy of M1 (likely referring to the D member; see below), but this does not seem adequate for our object: both the apparent magnitude and distance indicate that the primary (Ca) is a late F (F9; adopted by us). The only paper devoted to this subsystem in particular (see Section 3 of Hutchings et al. 2000) suggests that "thus, we conclude from the color differences that C and D have SpTy G0 and M2, respectively, with an uncertainty only on the order of one spectral subtype." Indeed, the photometry for Cb indicates an SpTy of G5–G6V, while the photometry for the D component indicates an M0.

HIP 43109 = SP1AB. This SB1 binary is the AB pair ($a = 0\farcs25$) of a quintuple system. It has a good orbital coverage, including historical data of lower precision and more recent interferometric data (including points in 2001.1, 2014.3, 2018.3, and 2021.2 from our survey), except near periastron. No data were included in SB9, but we recovered the original RV measurements from Adams (1939) and Underhill (1963), which encompass about one full revolution. This system has recently been observed with HARPS (Trifonov et al. 2020)[22] at 2004.1 (214 measurements), 2005.0 (one measurement), and 2005.2 (seven measurements).[23] The new RVs, with uncertainties below 0.01 km s^{-1}, greatly helped constrain the overall fit, which is shown in Figure 5. While the published SpTy differ, namely F8V in WDS and G1III in SIMBAD, the apparent magnitude and parallax render it more consistent with the primary being a giant G1III with a mass of 1.02 $M_\odot$ (adopted as prior). However, the MAP mass for the primary from our combined fits leads to a mass that is a factor of 2 larger, indicating it is a more massive and younger object (see Figure 6). Indeed, according to SIMBAD, it is known to be a fast rotator and variable, both characteristics being indicative of youth. A similar correction on ω and Ω with respect to the Orb6 values as found for HIP 5336 is seen in this system (see Table 2).

HIP 54061 = BU1077AB. Ours is the first combined orbit. This giant of SpTy G9III has a good orbital coverage, except for a short arc near periastron, where the small separation has

[22] https://vizier.u-strasbg.fr/viz-bin/VizieR?-source=J/A+A/636/A74

[23] Incidentally, in the notes to SB9 it is suggested that "High-dispersion observations have been continued at Victoria by C.D. Scarfe, and it should be possible soon to give a definitive spectroscopic orbit of this system."

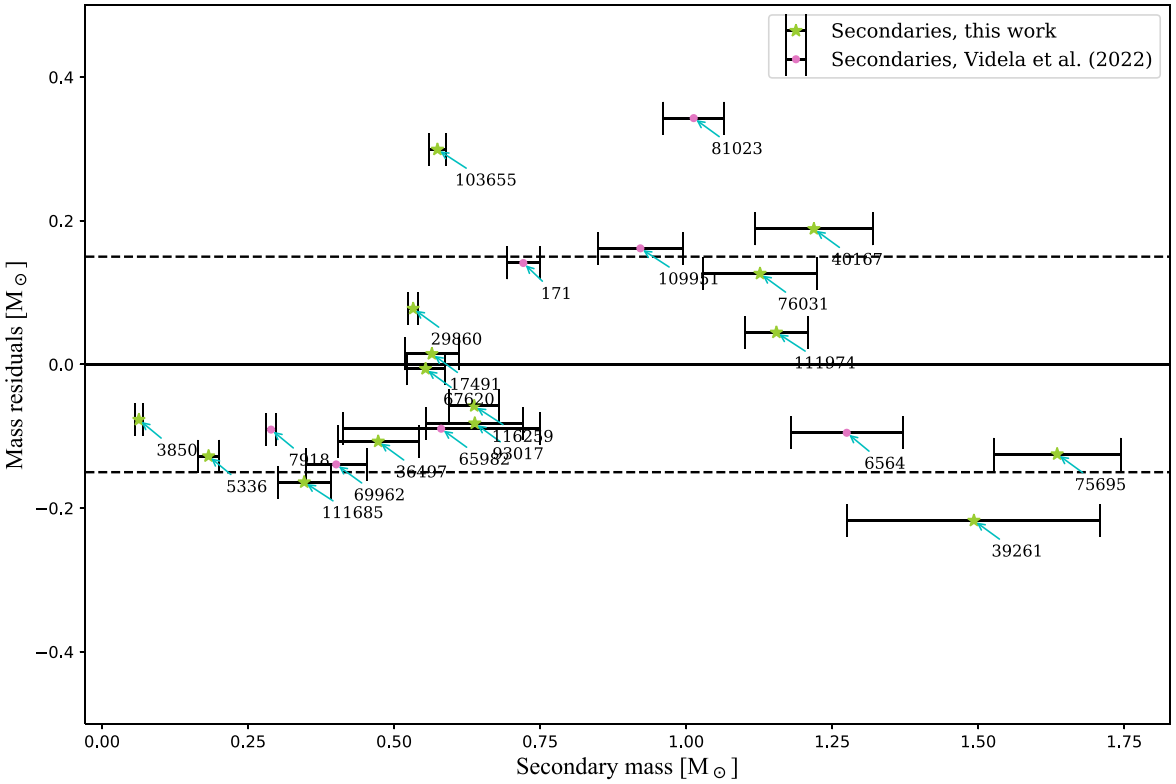

Figure 8. Mass residuals for the 22 class V secondaries of Figure 7 (including those from Videla et al. 2022), in comparison with the expected mass, given their luminosity from the fiducial relationships from Abushattal et al. (2020; their Table 18). The dashed lines indicate the empirical $\pm 1\sigma$ values, while the error on the mass in the abscissa comes from the upper and lower values presented in Table 2. The labels indicate the HIP numbers.

precluded so far a definitive resolution. The astrometric data include historical micrometric observations dating back to 1889, as well as interferometric data as recent as 2017. The RVs, which encompass one full orbit, are from the old work by Spencer Jones & Furner (1937) and have a rather large scatter. Initially, it was thought to have a very small inclination (fixed at 180° in the Hipparcos solution; see Söderhjelm 1999), but the inclination is now firmly determined: retrograde, at $167\overset{\circ}{.}2 \pm 2\overset{\circ}{.}1$ (see Table 2). The PDF for the mass indicates a larger mass ($2.7\,M_{\odot}$) than the input a priori value ($1.93\,M_{\odot}$ given its SpTy; see Table 1). As can be seen in Table 2 (fourth and fifth lines), this could be due to an erroneous parallax. Indeed, this object does not have a published parallax from Gaia, and the Hipparcos value has a rather large uncertainty. A purely astrometric mass sum of high quality has been obtained by Baines et al. (2018) with the Navy Precision Optical Interferometer, leading to $3.44 \pm 0.11\,M_{\odot}$. This value is consistent with our SB1 $+ p(m_1|\theta)$ solution, which gives $3.32 \pm 0.68\,M_{\odot}$, but it is very far from our SB1 $+ p(\varpi)$ solution, $5.7 \pm 1.6\,M_{\odot}$. This is puzzling, considering that they adopted the same Hipparcos parallax. Using both priors simultaneously, we obtained a mass sum of $5.32 \pm 0.57\,M_{\odot}$, i.e., 3.3σ larger than that derived by Baines et al. (2018). Of course, another possibility is that both WDS and SIMBAD are erroneous in the SpTy for the primary. The parallax and photometry indicate an earlier SpTy of B8–B9III, which, according Abushattal et al. (2020), would imply a mass of around $4\,M_{\odot}$, which is indeed close to our SB1 $+ p(\varpi)$ solution, which gives $3.8\,M_{\odot}$ for the primary (see Table 2). The scarcity and relatively low quality of the available RV data suggest that better coverage of the RV curve with modern spectrographs should help solve this puzzle. A similar correction on ω and Ω with respect to the Orb6 values as found for HIP 5336 is seen in this system (see Table 2).

HIP 55642 = STF1536AB. This is the tighter SB1 binary—AB—of a triple system. Abundant astrometry of relatively good quality, and covering the whole orbit, is available for this 184+ yr period system (it is the system with the longest period in our sample). Two interferometric observations from SOAR, at epochs 2018.3 and 2021.3, are included. No RV data are given in SB9, only in the references (Campbell & Moore 1928; Harper 1928; Petrie 1949; Abt & Levy 1976), from which we have extracted the RV data. To these, we have added 13 extra recent (2021.5–2022.3) high-precision RV measurements obtained with FIDEOS, which fit very well in the RV curve. Our adopted prior parallax is the unweighted average from Gaia Data Release 2 (DR2; there are no data for this object in DR3) for the AB and C components (separation of $5\overset{\prime}{.}5$). The SpTy reported is F4IV in WDS and F3V in SIMBAD, but the photometry and parallax indicate that the primary is a subgiant of type F0. We thus adopted the SpTy reported in WDS. Our systemic velocity of $-11.166 \pm 0.041\,\mathrm{km\,s^{-1}}$ is in reasonable agreement with the Gaia value at $-7.5 \pm 2.7\,\mathrm{km\,s^{-1}}$, especially considering the large formal uncertainty of the Gaia measurement.

HIP 67620 = WSI77. Pretty good coverage of the astrometric orbit. All but one data point are from our HRCam observations made with SOAR. Almost 1.5 revolutions are covered by the RV curve, including 24 recent data points from HARPS (Trifonov et al. 2020), at epochs

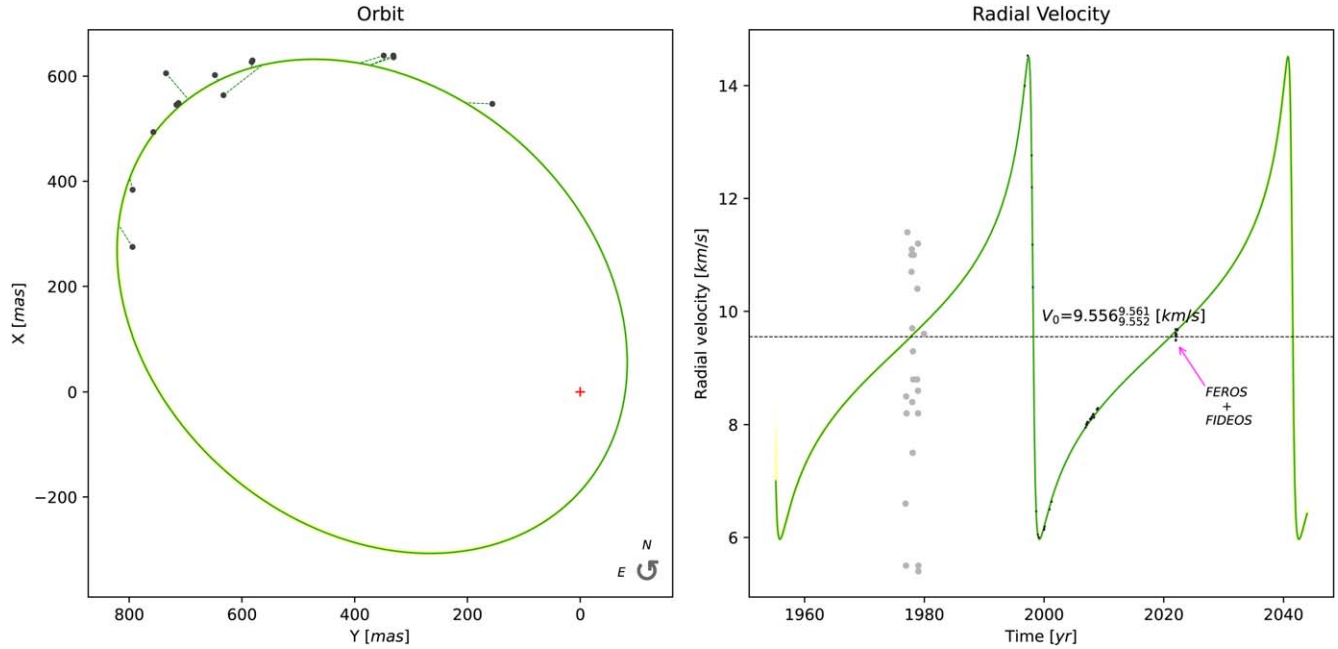

Figure 9. Similar to Figure 2, but for HIP 29860. For this system, the visual orbit is incomplete, with a severe lack of observations near periastron. Old RV data show a large scatter, while modern data and our own data from FEROS and FIDEOS (obtained in 2021 and 2022—indicated in the plot) are of much higher quality. This helped to constrain the final orbit, which, as indicated in Table 2, has a formal uncertainty of 0.3% in the period and 0.6% in the semimajor axis.

2012.2–2013.2, which match the orbit very well. The elements given in SB9 are from the spectroscopic-only study by Willmarth et al. (2016), but there is however a previous combined orbit + RV solution from Tokovinin (2012; given in the Orb6 line of the corresponding row in Table 2), which compares quite well with our values (see his Table 3). The solution from Tokovinin (2012) implies masses of $m_1 = 0.99\ M_\odot$ and $m_2 = 0.63\ M_\odot$, which are equivalent to our $m_1 = 0.917 \pm 0.048\ M_\odot$ and $m_2 = 0.554 \pm 0.043\ M_\odot$ given in Table 2. Our calculated systemic velocity is 5.361 ± 0.039 km s^{-1}. The Gaia value has a huge error (17 ± 23 km s^{-1}), which precludes a proper comparison. The Hipparcos and Gaia DR2 parallax (adopted by us as prior) differ quite substantially, being 53.88 ± 0.34 mas and 51.35 ± 0.4 mas, respectively. Our inferred MAP value is 53.10 ± 0.74 mas, closer to the Hipparcos parallax. There is no parallax in Gaia DR3 for this system (hence no RUWE either).

HIP 75695 = JEF1. Pretty good orbital coverage, including periastron. There are data of various quality, including interferometric measurements, the last of which are from our SOAR program (two data points at 2019.1). Historical (1930–1943) RV data of good quality, spanning one full orbit, are available from 1930 to 1943, and there are also earlier scattered data from 1902 to 1913 (Neubauer 1944), all of which fit the orbit quite well. While there is a parallax from Gaia DR3 (27.93 ± 0.97 mas, albeit with a large RUWE, 7.3), its formal error is 20% larger than that of Hipparcos (29.17 ± 0.76 mas), so we opted to use the Hipparcos value as a prior. Interestingly enough, our MAP parallax resulted in a value of 28.07 ± 0.44 mas (see Table 2), within less than 1σ of the Gaia value (see the PDF on the web page). While SIMBAD indicates a type F2V, and WDS A5V, the photometry and parallax are more consistent with an earlier type, so we adopted the WDS type as a prior. The combined orbit solution by Muterspaugh et al. (2010) gives $m_1 = 1.71 \pm 0.18\ M_\odot$ and $m_2 = 1.330 \pm 0.074\ M_\odot$, while we obtain slightly larger masses, $m_1 = 1.98 \pm 0.12\ M_\odot$ and $m_2 = 1.63 \pm 0.12\ M_\odot$, respectively. This is perhaps due to our smaller MAP parallax (they used the Hipparcos value). Of all the objects in our sample, this one has the largest measured metallicity, at [Fe/H] $\sim +1$, but its location in the MLR (indicated in Figure 7) coincides with that of the solar metallicity mean relationship.

HIP 76031 = TOK48. Ours is the first combined orbit. The orbital coverage of this tight pair ($P = 1.7$ yr, the shortest-period system in our sample) is poor, less than half the orbit. All data available are from our SOAR interferometry and cover epochs from 2009.3 to 2021.3 (15 data points). Due to the small separation, data are lacking near periastron, implying a relatively large uncertainty in the inclination ($i = 152.0 \pm 2.2°$). Fortunately, we have RVs of good quality covering several periods, which help to constrain the fit. We adopted as prior the Hipparcos parallax (19.67 ± 0.89 mas; this is the object in our sample with the largest parallax error, after HIP 111685), due to its smaller formal error (no parallax is given in Gaia DR3, while in DR2 it is 23.56 ± 1.2 mas). Our fitted MAP value for the orbital parallax resulted in a value of 21.18 ± 0.92 mas. Our fitted systemic velocity, 4.68 ± 0.37 km s^{-1}, disagrees slightly with the Gaia value at 6.2 ± 3.8 km s^{-1}, but note the large formal uncertainty of the Gaia measurement. Also, given the short period of the system, the Gaia value is not incompatible with the RV excursion from -2.5 km s^{-1} to about $+16$ km s^{-1} seen in the RV curve (see the figures on the web page).

HIP 78727 = STF1998AB. This SB1 binary is the inner system—AB—of a quintuple system. It has good coverage of the astrometric orbit since 1825, with data of various quality, including a few data points from our survey at epochs 2008, 2017, and 2019. There are no data in SB9, but we recovered old results from Campbell & Moore (1928) and

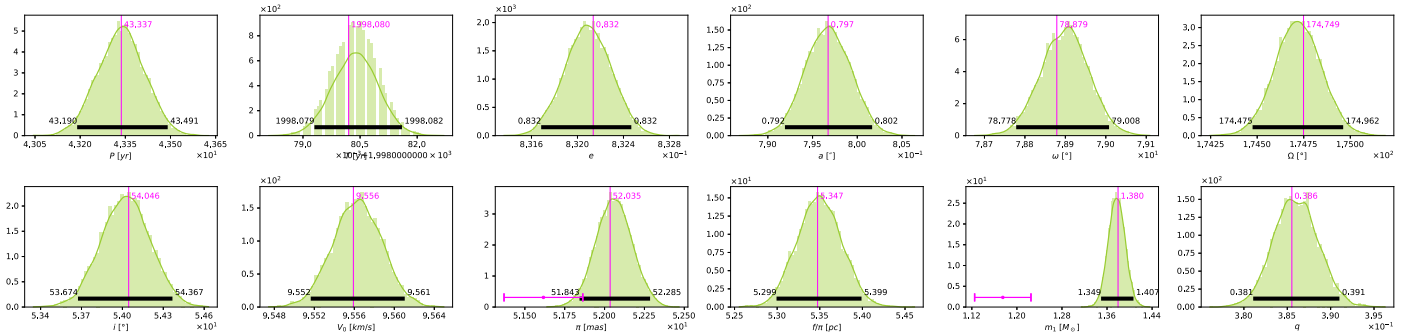

Figure 10. Same as Figure 4, but for the HIP 29860 binary system.

Chang (1929). Unfortunately, they cover less than a period and are of relatively low quality, as result of which our fitted value of V_0 is rather uncertain. In Gaia DR3, there is a double parallax: based on the coordinate, the first one in the catalog is for the C component and the second one is for the A component (the RUWE is nearly 1.3 in both cases—not that large). The value in Table 2 refers to the unweighted average of both. As for the SpTy, WDS lists the primary as F5IV, while SIMBAD gives F7V, but the parallax and photometry lead us to believe that the primary is a subgiant, thus we adopted F5IV as prior. Tokovinin (2020) has reported $m_1 = m_2 = 1.53\ M_\odot$, which is similar to, but slightly larger than our values of $m_1 = 1.404 \pm 0.042\ M_\odot$ and $m_2 = 1.383 \pm 0.054\ M_\odot$. As mentioned in the introduction to this section, this system exhibits periodic residuals after the MCMC orbital fit, most notably in position angle, with a peak-to-peak amplitude of about 14° (see Figure 11, top left panel) and a period comparable to that of the system itself (∼50 yr; top right panel). The trends are less evident in separation (middle panel) or RV (lower panel). It is unlikely that this is a perturbation to the Keplerian orbit induced by the C companion, located almost 8″ away (in comparison with the less than 1″ separation of the AB system), and with an estimated period of more than 1500 yr, according to the Tokovinin MSC catalog. The extant residuals may indicate the presence of an as yet unidentified third body in the AB system itself, an aspect that needs to be further investigated.

HIP 93017 = BU648AB. Ours is the first combined orbit. At a distance of almost 15 pc, this is the second-nearest SB1 system in our sample. It is the host of an exoplanet with a 2.8 yr period. The coverage of the visual orbit is quite complete, including periastron passage, and the data available are in general of good quality. The RVs obtained from the exoplanet campaign (see Duquennoy & Mayor 1991) cover only a tiny fraction of the orbit (the period of the binary is 61 yr), but this has been supplemented with newer data in Abt & Willmarth (2006a), downloaded from Abt & Willmarth (2006b), which cover 2001.5 to 2004.4 (see the data tables on the web page). There is good correspondence between our systemic velocity, $-45.97 \pm 0.11\ \mathrm{km\ s^{-1}}$, and that reported by Gaia DR3 at $-43.00 \pm 0.23\ \mathrm{km\ s^{-1}}$.

HIP 96302 = WRH32. Ours is the first combined orbit. This tight binary (separation of 25 mas) is the most compact system in our sample. At nearly 186 pc, it is the second most distant target in our sample. It has scarce astrometric data covering only one-half of the orbit, excluding periastron (where the separation becomes a few mas). It has plenty of RV observations covering several cycles, including old and new higher-precision data, hence the period is very well determined. There is a large discrepancy in the published values for the SpTy of the primary: A0V in WDS and G8III in SIMBAD. Its photometry and parallax are incompatible with both of these SpTy, predicting either a B6–7V or a B9III; in both cases, much more massive than our inferred value (indeed, see the SB1 + $p(\varpi)$ solution in Table 2). In the end, for our prior, SIMBAD's SpTy was adopted, based on the appearance and consistency of our MCMC corner plots for this solution. We note that, with a moderate RUWE of 1.5, the Hipparcos and Gaia values are consistent with each other, 5.37 ± 0.10 mas and 5.84 ± 0.31 mas, respectively, while our MAP orbital parallax is 5.46 ± 0.22 mas. The Hipparcos parallax was adopted as prior.

Our inferred mass values are somewhat different than the previously published values, with a more massive secondary; Martin et al. (1998) derive $3.344 \pm 1.165\ M_\odot$ and $1.586 \pm 0.612\ M_\odot$, whereas we obtain $2.61 \pm 0.32\ M_\odot$ and $2.50 \pm 0.33\ M_\odot$ for m_1 and m_2, respectively. Note the smaller errors of our combined solution. There is good correspondence between our systemic velocity, $-17.20 \pm 0.17\ \mathrm{km\ s^{-1}}$, and that reported by Gaia DR3 at $-15.8 \pm 1.9\ \mathrm{km\ s^{-1}}$.

HIP 103655 = KUI 103. This is a triple hierarchical system AaAb,B (AaAb is not resolved). Our solution refers only to the AB system, and we treat it as a binary. While AB is considered as an SB2 in SB9, it has only two measurements of the secondary component. As a result, our MCMC code was unable to converge to a reasonable binary solution, so we have decided to treat it as an SB1 until more data are secured for the B companion. It has coverage of about three-quarters of the astrometric orbit with data of reasonable quality. In RV, the phase coverage of the primary is only about one-half the orbit, near periastron. Pourbaix (2000) has published a combined solution, treating it as an SB2, but his solution is highly unreliable, the individual derived masses being $3.0 \pm 2.7\ M_\odot$ and $1.00 \pm 0.65\ M_\odot$. These masses are however incompatible with the SpTy of the primary being M2V, as indicated by both WDS and SIMBAD. These SpTy are furthermore consistent with the apparent magnitude and distance as derived from the Gaia DR3 parallax of 66.554 ± 0.072 mas (which in turn is also consistent with the Hipparcos parallax at 65.4 ± 1.8 mas, despite the large RUWE = 5.2). Our derived mass for the primary, $0.580 \pm 0.013\ M_\odot$, is somewhat larger than that implied from its SpTy ($0.43\ M_\odot$; from Abushattal et al. 2020). The same is true for the secondary, for which $q = 0.990 \pm 0.014\ M_\odot$, implying $0.574 \pm 0.015\ M_\odot$, while its apparent magnitude and parallax would suggest an SpTy for the secondary of M4–M5, with an implied mass of

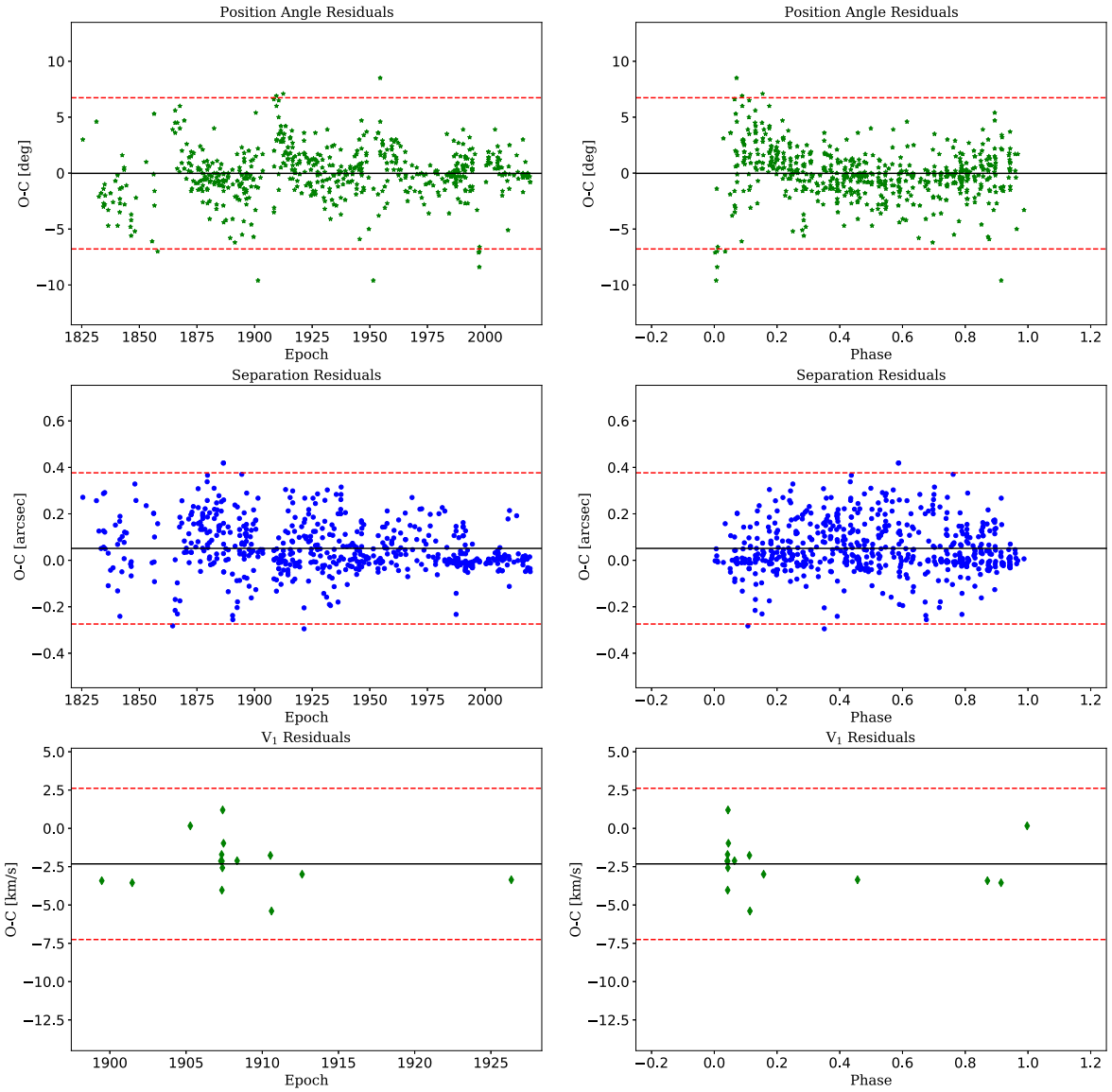

Figure 11. Residual O−C plots for HIP 78727, based on our MCMC solution with the orbital parameters indicated in Table 2. The dashed lines indicate the 3σ boundaries computed from the overall rms of each panel. There is a clear indication of a significant wobble in position angle, with a period of about 50 yr (top panel), possibly due to an accounted-for companion to the AB system (see the text for details). There are hints of some periodicity in the separation residuals as well (middle panel), but these are less significant. Scarce RV data preclude us from any conclusion based on the lower panel.

$0.24 - 0.31\,M_{\odot}$. We note, however, that both WDS and SIMBAD suggest an earlier type for the secondary, M0.5V (and a corresponding mass of about $0.5\,M_{\odot}$), in agreement with our result. This solution however poses a problem, because in the MLR, HIP 103655B is located far below the mean relationship (see Figure 7), which is because its mass ratio is almost 1, but the photometry indicates $\Delta m \sim 1.9$. We have no explanation for this discrepancy, but, despite these inconsistencies, we can conclude that our solution for this system is more reliable than that presented by Pourbaix (2000).

HIP 111685 = HDS3211AB. Not a lot of data are available, but they are well spread in both the orbital and RV phase coverage. There is a large discrepancy between the Hipparcos (51.2 ± 1.6 mas) and Gaia DR3 (46.89 ± 0.56 mas) parallaxes. This latter has a very large RUWE (32), which renders the Gaia solution somewhat questionable. Indeed, our solutions are more reliable and consistent adopting the Hipparcos parallax as prior (despite having the largest parallax uncertainty of our sample), leading to a MAP orbital parallax of 54.0 ± 1.4 mas, about 5σ larger than the Gaia value. While SB9 reports a combined solution, full orbital parameters are not provided in this catalog (see Table 2).

HIP 111974 = HO296AB. Very good coverage of the visual orbit, with abundant and well spread historical data, as well as newer higher-precision data. These includes 20 HRCam data points from our survey, between 2014.76 and 2019.86. No RV data are provided in SB9, so we extracted them from Batten et al. (1985). We note that while in this paper RV data for the companion are provided (which would place this system in the SB2 class), the authors do not use these data and treat it as an SB1 (see their Figure 1), probably because of the low precision of these latter data. No Gaia parallax is available, and we have used the Hipparcos value at 29.59 ± 0.68 mas as prior, leading to an inferred MAP

orbital parallax of 29.01 ± 0.50 mas. We have also treated this system as an SB1, and it provides an interesting test case of our single-line-with-priors methodology. Muterspaugh et al. (2010) obtained a combined SB2 solution for this system using a selected subsample of the Batten et al. (1985) RVs, leading to masses of $1.171 \pm 0.047\,M_{\odot}$ and $1.075 \pm 0.058\,M_{\odot}$, and an (orbital) distance of 34.43 ± 0.34 pc. This result compares quite well with our values, as can be seen from Table 2. In the notes to WDS, it says that "the primary is a giant, from isochrone fit" (no reference given), while both SIMBAD and WDS indicate a G4V, which is what we have adopted as prior. However, the parallax and photometry are more consistent with an earlier SpTy, F4–5V ($M_V \sim +3.5$), but certainly not a giant.

HIP 116259 = HDS3356. Our is the first combined orbit. This system has sparse but reasonable coverage of the visual orbit, except near periastron, and abundant good quality RV data covering the full phase space. It has a large RUWE value (8.1), and the Hipparcos (28.62 ± 0.95 mas) and Gaia DR3 (29.22 ± 0.15 mas) parallaxes differ by 0.6 mas. Our MAP orbital parallax is 29.08 ± 0.31 mas, i.e., within 1σ of the Gaia value. There is good correspondence between our systemic velocity, -3.310 ± 0.099 km s^{-1}, and that reported by Gaia DR3 at -1.30 ± 0.21 km s^{-1}, especially considering that the RV curve has excursions from -10 to $+3$ km s^{-1} (see the plot on the web page). It is interesting to note that Latham et al. (2002) obtained a binary mass function of $f(M) = 0.0774 \pm 0.0043 M_{\odot}$ from RVs alone, in perfect agreement with our predicted value from Table 2 of $0.0776\,M_{\odot}$.

5. Conclusions and Final Comments

Applying a Bayesian method developed by our group, we have obtained mass ratio estimates for 22 SB1s with available astrometric and RV data, using as priors the SpTy of the primary and the trigonometric parallax of the system. For nine previously unstudied systems, we present, for the first time, a combined orbital solution and uncertainty estimates based on a Bayesian approach. We have made an exhaustive comparison of our results with previous studies, finding a very good agreement. This includes a comparison of our systemic velocities with Gaia RVs. We have combined the present results with those from a previous study by Videla et al. (2022), for systems of luminosity class V covering a mass range $0.6 \leqslant M_{\odot} \leqslant 2.5$ to construct a pseudo MLR based on 23 systems (45 stars). We find good correspondence with previously determined MLRs based on SB2 systems, proving the usefulness of our method. Although some inconsistencies have been found, when the next Gaia data releases are available (with an improved treatment of binary systems), the parallaxes will become more reliable and some discrepancies could disappear. An effort is being made by our team to obtain high-signal-to-noise-ratio, low-resolution spectra for these (bright) binaries, so that their SpTy and luminosity class are firmly established. This will open up a path to utilizing SB1s for more refined studies of the MLR, using larger samples.

Acknowledgments

We would like to thank an anonymous referee as well as the scientific and statistic editors of the journal for a careful reading of our manuscript, and for their several very useful comments that significantly contributed to the readability of our paper.

R.A.M. and E.C. acknowledge funding from the Vicerrectoria de Investigacion y Desarrollo (VID) of the Universidad de Chile, project: ENL02/23. R.A.M. acknowledges the European Southern Observatory in Chile for its hospitality during a period of sabbatical leave in which this work was finished. L.V. acknowledges support for FIDEOS operation from FONDECYT/ANID grant No. 1211162 and Quimal ASTRO20-0025.

We are grateful to Andrei Tokovinin (CTIO/NOIRLab) for his help and support with the use of HRCam at SOAR. We also acknowledge all the support personnel at CTIO for their commitment to operations during the difficult COVID times.

This research has made use of the Washington Double Star Catalog maintained at the U.S. Naval Observatory and of the SIMBAD database, operated at CDS, Strasbourg. We are very grateful for the continuous support of the Chilean National Time Allocation Committee under programs CN2018A-1, CN2019A-2, CN2019B-13, CN2020A-19, CN2020B-10, CN2021B-17, CN2022A-11, CN2022B-14, and CN2023A-7 for SOAR and CN2022A-1, CN2022B-8, and CN2023A-5 for FEROS. This research has made use of the VizieR catalogue access tool, CDS, Strasbourg, France (DOI : 10.26093/cds/vizier). The original description of the VizieR service was published in 2000, A&AS 143, 23.

Facility: AURA: SOAR

ORCID iDs

Rene A. Mendez https://orcid.org/0000-0003-1454-0596
Miguel Videla https://orcid.org/0000-0002-7140-0437
Edgardo Costa https://orcid.org/0000-0003-4142-1082

References

Abt, H. A., & Levy, S. G. 1976, ApJS, 30, 273
Abt, H. A., & Willmarth, D. 2006a, ApJS, 162, 207
Abt, H. A., & Willmarth, D. 2006b, yCat, J/ApJS/162/207
Abushattal, A. A., Docobo, J. A., & Campo, P. P. 2020, AJ, 159, 28
Adams, B. 1939, PASP, 51, 116
Agati, J. L., Bonneau, D., Jorissen, A., et al. 2015, A&A, 574, A6
Anguita-Aguero, J., Mendez, R. A., Clavería, R. M., & Costa, E. 2022, AJ, 163, 118
Baines, E. K., Armstrong, J. T., Schmitt, H. R., et al. 2018, AJ, 155, 30
Balega, I. I., Balega, Y. Y., & Malogolovets, E. V. 2004, in The A-Star Puzzle, ed. J. Zverko et al. (Cambridge: Cambridge Univ. Press), 683
Balega, Y. Y., Tokovinin, A. A., Pluzhnik, E. A., & Weigelt, G. 2002, AstL, 28, 773
Batten, A. H., Lu, W., & Scarfe, C. D. 1985, JRASC, 79, 167
Beavers, W. I., & Eitter, J. J. 1986, ApJS, 62, 147
Bond, H. E., Schaefer, G. H., Gilliland, R. L., & VandenBerg, D. A. 2020, ApJ, 904, 112
Brahm, R., Jordán, A., & Espinoza, N. 2017, PASP, 129, 034002
Campbell, W. W., & Moore, J. H. 1928, Pub. Lick Obs., 16, 234
Carrier, F., North, P., Udry, S., & Babel, J. 2002, A&A, 394, 151
Catala, C., Forveille, T., & Lai, O. 2006, AJ, 132, 2318
Chang, Y. C. 1929, ApJ, 70, 182
Duquennoy, A., & Mayor, M. 1991, A&A, 248, 485
Fekel, F. C., & Scarfe, C. D. 1986, AJ, 92, 1162
Harper, W. 1928, Publication of the Dominion Astrophysical Observatory, Vol. 6, 151
Hutchings, J. B., Griffin, R. F., & Ménard, F. 2000, PASP, 112, 833
Katoh, N., Itoh, Y., Toyota, E., & Sato, B. 2013, AJ, 145, 41
Katz, D., Sartoretti, P., Guerrier, A., et al. 2023, A&A, 674, A5
Kaufer, A., Stahl, O., Tubbesing, S., et al. 1999, Msngr, 95, 8
Latham, D. W., Stefanik, R. P., Torres, G., et al. 2002, AJ, 124, 1144
Malkov, O. Y., Tamazian, V. S., Docobo, J. A., & Chulkov, D. A. 2012, A&A, 546, A69

Martin, C., Mignard, F., Hartkopf, W. I., & McAlister, H. A. 1998, A&AS, 133, 149
Mason, B. D. 2015, IAUGA, 29, 2300709
Mason, B. D., Wycoff, G. L., Hartkopf, W. I., Douglass, G. G., & Worley, C. E. 2001, AJ, 122, 3466
Mayor, M., Pepe, F., Queloz, D., et al. 2003, Msngr, 114, 20
Mendez, R. A., Claveria, R. M., Orchard, M. E., & Silva, J. F. 2017, AJ, 154, 187
Muterspaugh, M. W., Hartkopf, W. I., Lane, B. F., et al. 2010, AJ, 140, 1623
Neubauer, F. J. 1944, ApJ, 99, 134
Parsons, S. B. 1983, ApJS, 53, 553
Peretti, S., Ségransan, D., Lavie, B., et al. 2019, A&A, 631, A107
Petrie, R. 1949, PDAO, 8, 117
Pourbaix, D. 2000, A&AS, 145, 215
Pourbaix, D., Tokovinin, A. A., Batten, A. H., et al. 2004, A&A, 424, 727
Riddle, R. L., Tokovinin, A., Mason, B. D., et al. 2015, ApJ, 799, 4
Sahlmann, J., Ségransan, D., Queloz, D., et al. 2011, A&A, 525, A95
Scarfe, C. D., Barlow, D. J., & Fekel, F. C. 2000, AJ, 119, 2415
Scholz, G., & Lehmann, H. 1988, AN, 309, 33
Skiff, B. A. 2014, yCat, B/mk
Söderhjelm, S. 1999, A&A, 341, 121
Spencer Jones, H., & Furner, H. H. 1937, MNRAS, 98, 92
Straižys, V., & Kuriliene, G. 1981, Ap&SS, 80, 353
Struve, O., & Huang, S. S. 1958, in Handbuch der Physik, ed. S. Flügge, Vol. 50 (Berlin: Springer), 243
Tokovinin, A. 2012, AJ, 144, 56
Tokovinin, A. 2018, ApJS, 235, 6
Tokovinin, A. 2020, AJ, 159, 265
Tokovinin, A. 2022, AJ, 163, 161
Tokovinin, A., Mason, B. D., Mendez, R. A., Costa, E., & Horch, E. P. 2020, AJ, 160, 7
Tokovinin, A. A. 1997, A&AS, 124, 75
Trifonov, T., Tal-Or, L., Zechmeister, M., et al. 2020, A&A, 636, A74
Underhill, A. B. 1963, PDAO, 12, 159
Unwin, S. C., Shao, M., Tanner, A. M., et al. 2008, PASP, 120, 38
Vanzi, L., Zapata, A., Flores, M., et al. 2018, MNRAS, 477, 5041
Videla, M., Mendez, R. A., Clavería, R. M., Silva, J. F., & Orchard, M. E. 2022, AJ, 163, 220
Vogt, S. S., Butler, R. P., Marcy, G. W., et al. 2002, ApJ, 568, 352
Wenger, M., Ochsenbein, F., Egret, D., et al. 2000, A&AS, 143, 9
Willmarth, D. W., Fekel, F. C., Abt, H. A., & Pourbaix, D. 2016, AJ, 152, 46